Title
Cleaning up translation failures: how Ribosome-associated Quality Control maintains cellular proteostasis

Author
Hickey, Kelsey

Publication Date
2020

Peer reviewed|Thesis/dissertation

Cleaning up translation failures: how Ribosome-associated Quality Control maintains cellular proteostasis

by
Kelsey Hickey

DISSERTATION
Submitted in partial satisfaction of the requirements for degree of
DOCTOR OF PHILOSOPHY

in

Biochemistry and Molecular Biology

in the

GRADUATE DIVISION
of the
UNIVERSITY OF CALIFORNIA, SAN FRANCISCO

Approved:

DocuSigned by:
Jonathan Weissman
A16A9953185F4C9...

Jonathan Weissman
Chair

DocuSigned by:
David Toczyski
DocuSigned by:
Davide Ruggero
14C3B6AD60C5446...

David Toczyski

Davide Ruggero

Committee Members

Acknowledgements

This work would not be possible without the support and contributions of many people.

First, I would like to thank my mentor, Jonathan Weissman for constant support and creativity. He has allowed me the freedom to explore my own ideas, and when necessary helped me to focus and push my project forward.

I want to thank both current and past Weissman lab members. This work would not have been possible without support from the entire lab. In particular, I would like to thank Kamena Kostova for her mentorship. She was always patient, and I am very thankful to have had the opportunity to learn from her. I want to thank Marco Jost and Matt Shurtleff for feedback on proposals, papers and experimental design. Jeff Hussmann and Marco Jost have been an amazing resource to learn data analysis. Thanks to Matt Shurtleff, Lakshmi Miller-Vedam and Zach Cogan for always making the time for a meeting.

I want to thank my thesis committee members David Toczyski and Davide Ruggero for their constant guidance and support on my PhD project and for helping me to discover my ongoing scientific interests.

I would like to thank my friends both old and new who made graduate school possible. In particular I am thankful for both of my hockey teams, Club Cindy and No Name.

I want to thank my family for their love and support. My parents have always encouraged me to peruse my dreams and have provided me with every opportunity possible.

Finally, I want to thank my partner, Arda Mizrak, for his endless support. I have learned so much from him both scientifically and personally. I couldn't be happier that grad school brought us together.

The material in this dissertation is reproduced from a peer-reviewed published article (Kostova K, Hickey KL, Osuna BA, Hussmann JA, Frost A, Weinberg DE, Weissman, JS. **CAT-tailing as a fail-safe mechanism for efficient degradation of stalled nascent polypeptides.** *Science* 357, 414-417 (2017)) and a preview of an article currently in revision (Hickey KL, Dickson K, Cogan JZ, Replogle JM, Schoof M, D'Orazio KN, Sinha NK, Hussmann JA, Jost M, Frost A, Green R, Kostova K, Weissman JS. **GIGYF2 and 4EHP Inhibit Translation Initiation of Defective Messenger RNAs to Assist Ribosome-Associated Quality Control.** (2020). *biorxiv: doi.org/10.1101/792994*). Jonathan Weissman directed and supervised the research in this dissertation.

Cleaning up translation failures: how Ribosome-associated Quality Control maintains cellular proteostasis

Kelsey Hickey

ABSTRACT

Ribosome-associated Quality Control (RQC) pathways protect cells from toxicity caused by incomplete protein products resulting from translation of damaged or problematic mRNAs. One component of the RQC pathway, Ltn1p, is an E3 ubiquitin ligase that targets partially synthesized polypeptides for ubiquitin-proteasome mediated degradation. A second core RQC component, Rqc2p, not only nucleates the complex formation but also modifies the nascent polypeptide by adding a carboxyl-terminal alanine and threonine (CAT) tail through a noncanonical elongation reaction. We found that Ltn1p can efficiently access only nascent-chain lysines immediately proximal to the ribosome exit tunnel. For substrates without Ltn1p-accessible lysines, CAT-tailing by Rqc2p expanded the range of RQC-degradable substrates by exposing lysines sequestered in the ribosome exit tunnel.

Although the core RQC factors are conserved from yeast to human, much less is known about the mammalian counterparts. Interestingly, the phenotypes observed with loss of RQC in mammals are more severe and include cytotoxicity at a cellular level, and neurodegeneration at an organismal level. Due to the increased requirement for RQC in mammals, we used CRISPR-Cas9-based screening to search for additional RQC strategies in mammals. We found that failed translation leads to specific inhibition of translation initiation on that message. This negative feedback loop is mediated by two translation inhibitors, GIGYF2 and 4EHP. Both model substrates and growth-based assays established that inhibition of additional rounds of translation

acts in concert with known RQC pathways to prevent buildup of toxic proteins. Inability to block translation of faulty mRNAs, and subsequent accumulation of partially synthesized polypeptides, could explain the neurodevelopmental and neuropsychiatric disorders observed in mice and humans with compromised GIGYF2 function.

Table of Contents

List of Figures

List of Tables

1. INTRODUCTION

Translation is an enormous amplification step in which each messenger RNA (mRNA) is turned into hundreds of proteins. Defective mRNAs lacking a stop codon due to premature polyadenylation or mRNAs harboring damage, non-optimal codons or RNA structure can cause ribosomes to stop translating before they reach a stop codon (Doma and Parker, 2006; Klauer and van Hoof, 2012; Letzring et al., 2013). Such stalled ribosomes pose numerous threats to the cells as they decrease protein output from an mRNA, block translation by trailing ribosomes, and carry incomplete polypeptide that can aggregate or exhibit dysregulated activity (Choe et al., 2016; Chu et al., 2009; Yonashiro et al., 2016a). Therefore, if ribosome stalling is not detected and resolved, it can jeopardize cell and organismal viability.

To counter the threat posed by stalled ribosomes, cells possess multiple surveillance mechanisms, collectively referred to here as Ribosome-associated Quality Control (RQC) pathways. Recent studies have shown that one of the earliest events that can initiate RQC is the collision between the stalled ribosome and a trailing one (Juszkiewicz and Hegde, 2017; Juszkiewicz et al., 2018; Simms et al., 2017a; Sundaramoorthy et al., 2017). One mechanism of detection of such collided disomes is mediated by an E3 ubiquitin ligase Hel2p (ZNF598 in human) (Brandman et al., 2012; Garzia et al., 2017; Juszkiewicz et al., 2018; Letzring et al., 2013; Matsuo et al., 2017; Saito et al., 2015; Shao et al., 2015; Sundaramoorthy et al., 2017). After detection, the stalled ribosome is dissociated by the combined action of Dom34p/ Hbs1p (Izawa et al., 2012) and the RQC-Trigger complex (Hashimoto et al., 2020; Matsuo et al., 2017). The 60S ribosome, which still carries the stalled nascent polypeptide, recruits the core RQC complex components, allowing the nascent polypeptide to be ubiquitinated and extracted from

the exit tunnel for proteasomal degradation (Bengtson and Joazeiro, 2010; Brandman et al., 2012; Kostova et al., 2017; Osuna et al., 2017).

The RQC complex in *Saccharomyces cerevisiae* comprises Rqc1p, Rqc2p, the E3 ubiquitin ligase Ltn1p, and Cdc48p. Rqc2p acts to both recruit Ltn1p and to facilitate tagging of partially synthesized polypeptides with a Carboxy-terminal Alanine and Threonine (CAT) tail in a non-canonical elongation reaction (CAT-tailing) (Shen et al., 2015). Previous studies established that CAT-tails facilitate protein aggregation when RQC-mediated degradation is compromised, leading to chaperone sequestration and proteotoxic stress (Choe et al., 2016; Defenouillère et al., 2016; Yonashiro et al., 2016b). However, an Rqc2p mutant defective in CAT-tailing ($Rqc2p^{mut}$) fully supports Ltn1p-dependent degradation of the limited number of stalling substrates studied so far (Choe et al., 2016; Defenouillère et al., 2016; Shen et al., 2015; Yonashiro et al., 2016b). We found that the biological role of CAT-tailing in the context of a functional RQC is to expose hidden lysines from the exit tunnel, thus expanding the number of substrates which can be ubiquitinated by Ltn1p and subsequently degradation.

These quality control pathways have been discovered and extensively studied in yeast. However, far less is known about their conserved counterparts in mammals. In contrast to yeast, where loss of core RQC factors is well tolerated under standard growth conditions, mutations in the mammalian factors affect cell growth and have been associated with complex disease. For example, partial loss-of-function mutations in LTN1, the ubiquitin ligase facilitating the degradation of the stalled nascent polypeptide, cause neurodegeneration in mice (Bengtson and Joazeiro, 2010; Chu et al., 2009). Together, these observations further emphasize the importance of RQC for maintaining protein homeostasis in higher eukaryotes (Brandman et al., 2012; Defenouillère et al., 2013; Shao and Hegde, 2014; Shao et al., 2013; Verma et al., 2013). Given

the toxicity of partially synthesized proteins, it is possible that multiple layers of regulation exist to prevent, detect, and cope with ribosome stalling. However, our understanding of how the RQC cooperates with other pathways governing protein homeostasis is incomplete. Here we use reporter-based and growth-based genome-wide CRISPRi screens (Gilbert et al., 2014; Qi et al., 2013) to systematically characterize the mammalian RQC pathway. We identify a new branch of the RQC that involves two factors, GIGYF2 and 4EHP, that block ribosome initiations on problematic mRNAs.

2. RESULTS

2.1. RQC substrates require lysine residues to be degraded

In eukaryotic cells, when translation fails (e.g., due to a faulty mRNA or ribosome stalling) the incomplete nascent chain is targeted for proteasomal degradation (Ito-Harashima et al., 2007) by a conserved ribosome-associated quality control pathway (Brandman and Hegde, 2016). This process involves disassociation of the mRNA and 40S subunit followed by recruitment of the Ribosome-associated Quality Control (RQC) complex (Brandman et al., 2012; Defenouillère et al., 2013; Shao and Hegde, 2014; Shao et al., 2013; Verma et al., 2013) to the 60S subunit-nascent chain complex (Fig. 1). The RQC complex in *Saccharomyces cerevisiae* comprises Rqc1p, Rqc2p, the E3 ubiquitin ligase Ltn1p, and Cdc48p. Rqc2p acts to both recruit Ltn1p and to facilitate tagging of partially synthesized polypeptides with a Carboxy-terminal Alanine and Threonine (CAT) tail in a non-canonical elongation reaction (CAT-tailing) (Fig. 1) (Shen et al., 2015). Previous studies established that CAT-tails facilitate protein aggregation when RQC-mediated degradation is compromised, leading to chaperone sequestration and proteotoxic stress (Choe et al., 2016; Defenouillère et al., 2016; Yonashiro et al., 2016b). However, an Rqc2p mutant defective in CAT-tailing ($Rqc2p^{mut}$) fully supports Ltn1p-dependent degradation of the limited number of stalling substrates studied so far (Choe et al., 2016; Defenouillère et al., 2016; Shen et al., 2015; Yonashiro et al., 2016b). Thus, the biological role of CAT-tailing in the context of a functional RQC remains undefined.

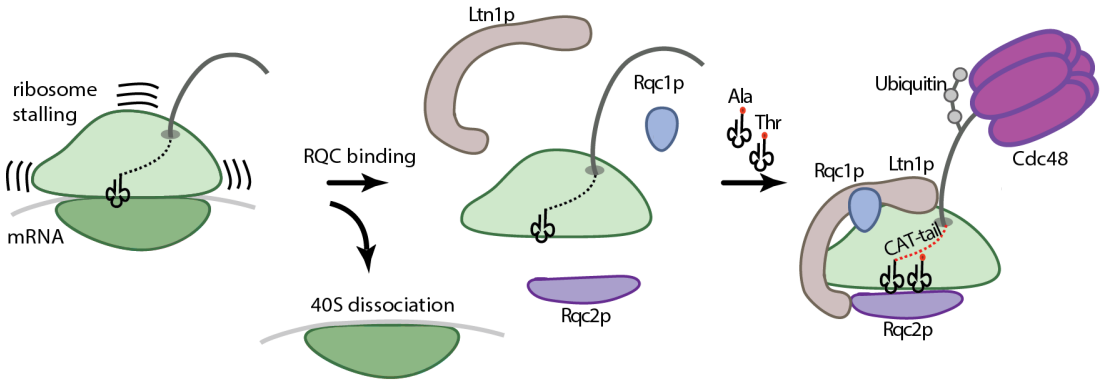

Figure 1. RQC pathway in yeast. Model for RQC-mediated degradation of nascent polypeptides.

To investigate the role of CAT-tailing in nascent polypeptide degradation, we designed two stalling constructs (GFP_{20Lys} and $GFP_{Lys\text{-}free}$) that differed in whether or not they encoded lysines, the canonical ubiquitin acceptor (Fig. 2B, C). Both constructs contained a poly-arginine track (R12) that efficiently blocked translation (Dimitrova et al., 2009; Letzring et al., 2010). The resulting GFP_{20Lys} nascent polypeptide was degraded in an RQC-dependent manner (Fig. 2B). In *ltn1Δ* cells, we detected higher molecular weight CAT-tailed species, which collapsed into a discrete band upon removal of C-terminal extensions by TEV protease treatment (Fig. 2B, middle panel). Finally, consistent with previous work (Shen et al., 2015), GFP_{20Lys} was efficiently degraded in the CAT-tailing deficient $rqc2^{mut}$ strain, confirming that CAT-tails are not necessary for degradation of this substrate (Fig. 2B).

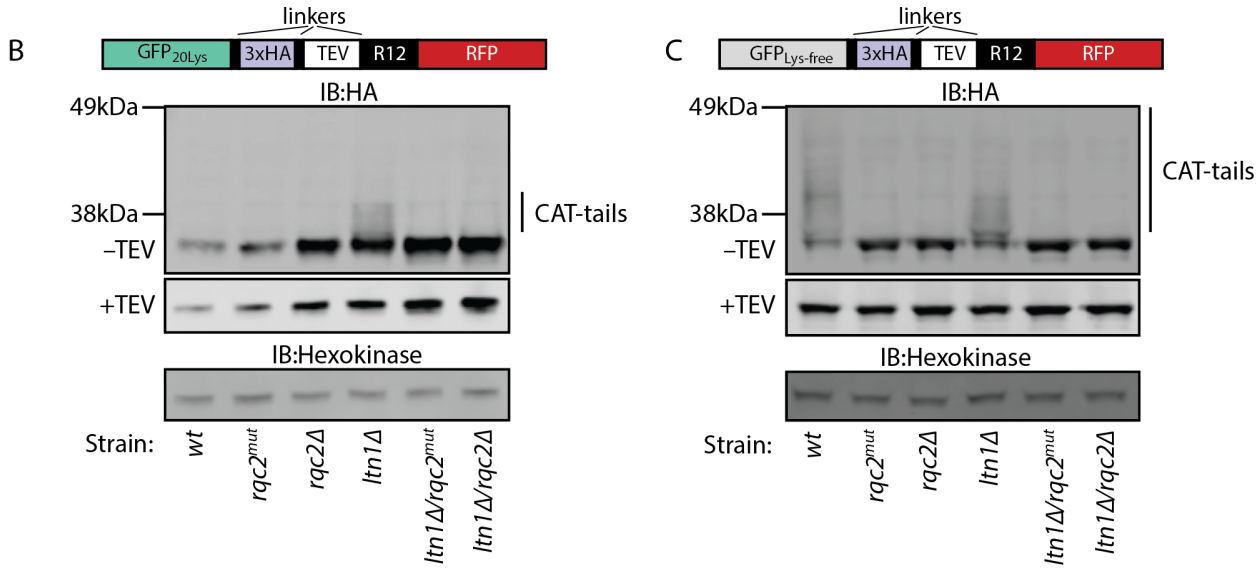

Figure 2. Degradation of RQC substrates requires lysines. (**B, C**) Immunoblots (IBs) of stalling reporters with or without lysines in RQC deletion strains.

In contrast to GFP_{20Lys}, $GFP_{Lys\text{-}free}$ was heavily CAT-tailed even in wild-type (*wt)* cells (Fig. 2C), consistent with previous reports (Yonashiro et al., 2016b). However, these CAT-tails did not trigger degradation, since comparable amounts of $GFP_{Lys\text{-}free}$ accumulated in *wt* cells and RQC deletions strains (Fig. 2C). This indicates that CAT-tails do not function as degrons, as their addition alone is not enough for RQC mediated degradation.

2.2. Direct Ltn1p ubiquitination mediates RQC substrate degradation

Cryo-electron microscopy structures of Ltn1p bound to the 60S subunit have revealed that the RING domain of Ltn1p, which is required for ubiquitin transfer, is held in close proximity to the ribosome exit tunnel (Lyumkis et al., 2014; Malsburg et al., 2015). Thus, the position of lysines along the nascent polypeptide may determine the ability of Ltn1p to ubiquitinate them. To further explore this idea, we designed stalling constructs with four lysines in an unstructured region (3xFLAG tag) that were systematically displaced from the R12 stalling site by 0, 10, 20, 40, or 80 amino acids of neutral XTEN linker (Schellenberger et al., 2009) (XTEN0-80, respectively) (Fig. 3). For these constructs, the four lysines will be either sequestered in (XTEN0), emerging from (XTEN10, XTEN20), or past (XTEN40, XTEN80) the ribosome exit tunnel. Initially, we used the relative degradation of the constructs as a proxy for Ltn1p's ability to ubiquitinate the lysines.

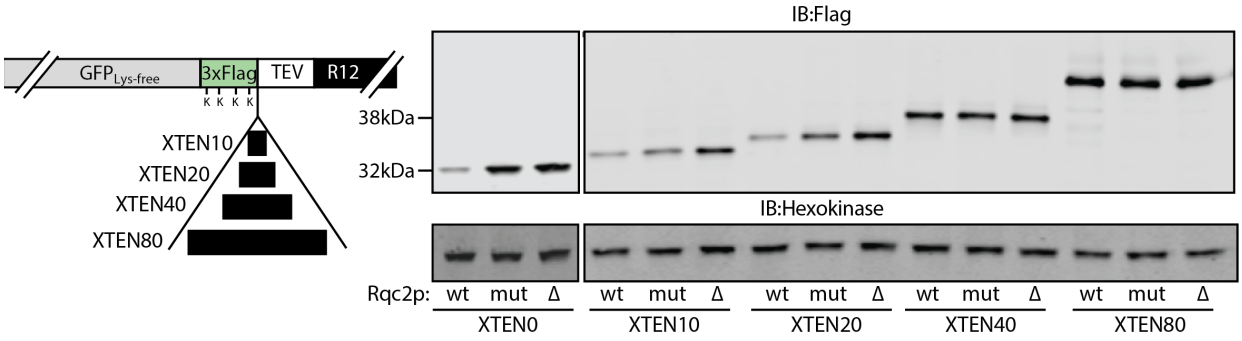

Figure 3. Lysine positioning is critical for proteasomal degradation. Scheme of constructs used (left), IB of TEV-treated XTEN constructs (right).

In contrast to previous RQC substrates (Shen et al., 2015), XTEN0 was efficiently degraded only in cells capable of CAT-tailing in an Ltn1p-dependent manner (Fig. 3). These data argue that CAT-tail elongation pushes sequestered lysines out of the exit tunnel making them available for Ltn1p-mediated ubiquitination, as hypothesized (Brandman and Hegde, 2016; Simms et al., 2017b). Compared to XTEN0, degradation of XTEN10 and XTEN20 became less dependent on CAT-tailing (Fig. 3). Critically, when the lysines were positioned past a certain distance (XTEN40 and XTEN80), the substrates were completely resistant to RQC-mediated degradation.

To ensure that the observed degradation was mediated through the direct ubiquitination of nascent chains by Ltn1p, we developed an *in vivo* ubiquitin assay. First, GFP_{20Lys} was expressed, followed by immunoprecipitation using the encoded 3xFLAG tag. Myc-tagged ubiquitin was co-expressed, and cells were treated with MG132 to inhibit proteasome mediated degradation. These constructs were analyzed for ubiquitinated species (Myc-ubiquitin) by western blot (Fig. 4A). We found that we could successfully detect ubiquitinated species both in the cell lysate, and well as specifically on GFP_{20Lys} after immunoprecipitation. Rqc2p and Ltn1p were essential for this ubiquitination of $GFP_{20Lys,}$ but CAT-tails were not, as $Rqc2p^{mut}$ strain lead to similar ubiquitin signal on GFP_{20Lys} (Fig. 4B). After establishing this system, we measured the direct ubiquitination of the XTEN constructs to ensure that observed degradation was mediated through Ltn1p activity.

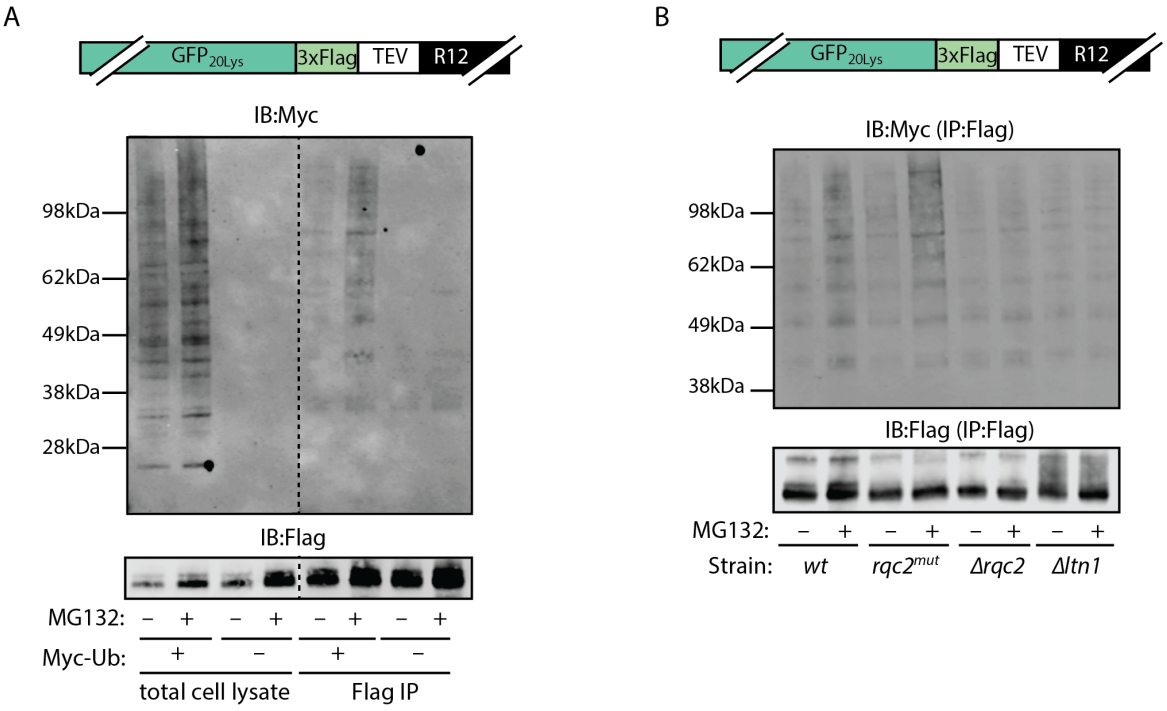

Figure 4. Ubiquitin can be detected on the GFP$_{20Lys}$ stalling substrate. (**A**) *pdr5Δ* cells expressing GFP$_{20Lys}$ stalling reporter and copper-inducible Myc-tagged ubiquitin were treated with (+) or without (-) Cu_2SO_4. Samples from total cell lysate or denaturing immunoprecipitation (Flag IP) were analyzed on SDS-PAGE and IB. (**B**) Cells expressing Myc-tagged ubiquitin and GFP$_{20Lys}$ stalling reporter were treated with (+) or without (-) the proteasome inhibitor MG132. SDS-boiled lysates from wt, *rqc2^{mut}*, *rqc2Δ,* and *ltn1Δ* cells were used for Flag IP. The eluate was analyzed by SDS-PAGE and IB. All cells had the multidrug transporter gene *PDR5* deleted to facilitate MG132 accumulation.

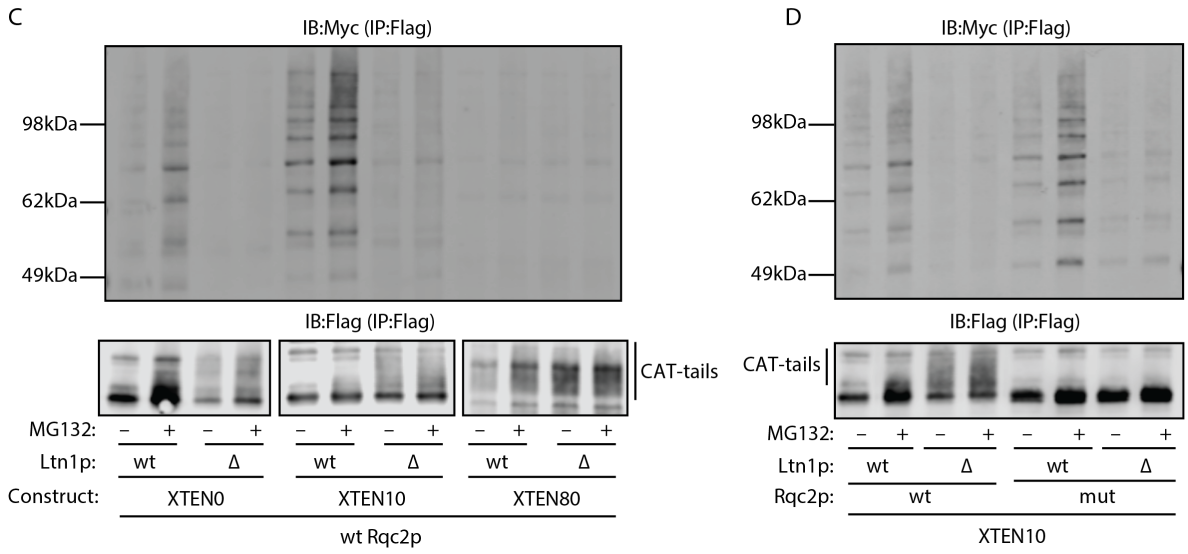

Figure 5. Lysine positioning is critical for Ltn1p-mediated ubiquitination and proteasomal degradation. (**C, D**) Denaturing immunoprecipitation (Flag IP) of XTEN 0, 10, and 80 stalling constructs from cells expressing Myc-tagged ubiquitin.

Consistent with these degradation results, we observed Ltn1p-dependent ubiquitination of XTEN constructs when lysines were positioned in the exit tunnel or within the Ltn1p-accessible region, and no ubiquitination was observed when the lysines were past the Ltn1p-accessible window (Fig. 5C, 6A-D). In wild-type Rqc2p cells, XTEN0 and XTEN10 were both efficiently ubiquitinated in an Ltn1p-dependent manner. In contrast, XTEN80 was not ubiquitinated by Ltn1p or degraded by RQC. (Fig. 5C, 6A-D). In addition, we observed similar levels of ubiquitination in cells expressing wild-type or mutant Rqc2p (Fig. 5D). Taken together, these data support a model in which Ltn1p can only access a limited window of amino acids on the nascent polypeptide and that the process of CAT-tailing enables Ltn1p to gain access to lysines sequestered in the exit tunnel.

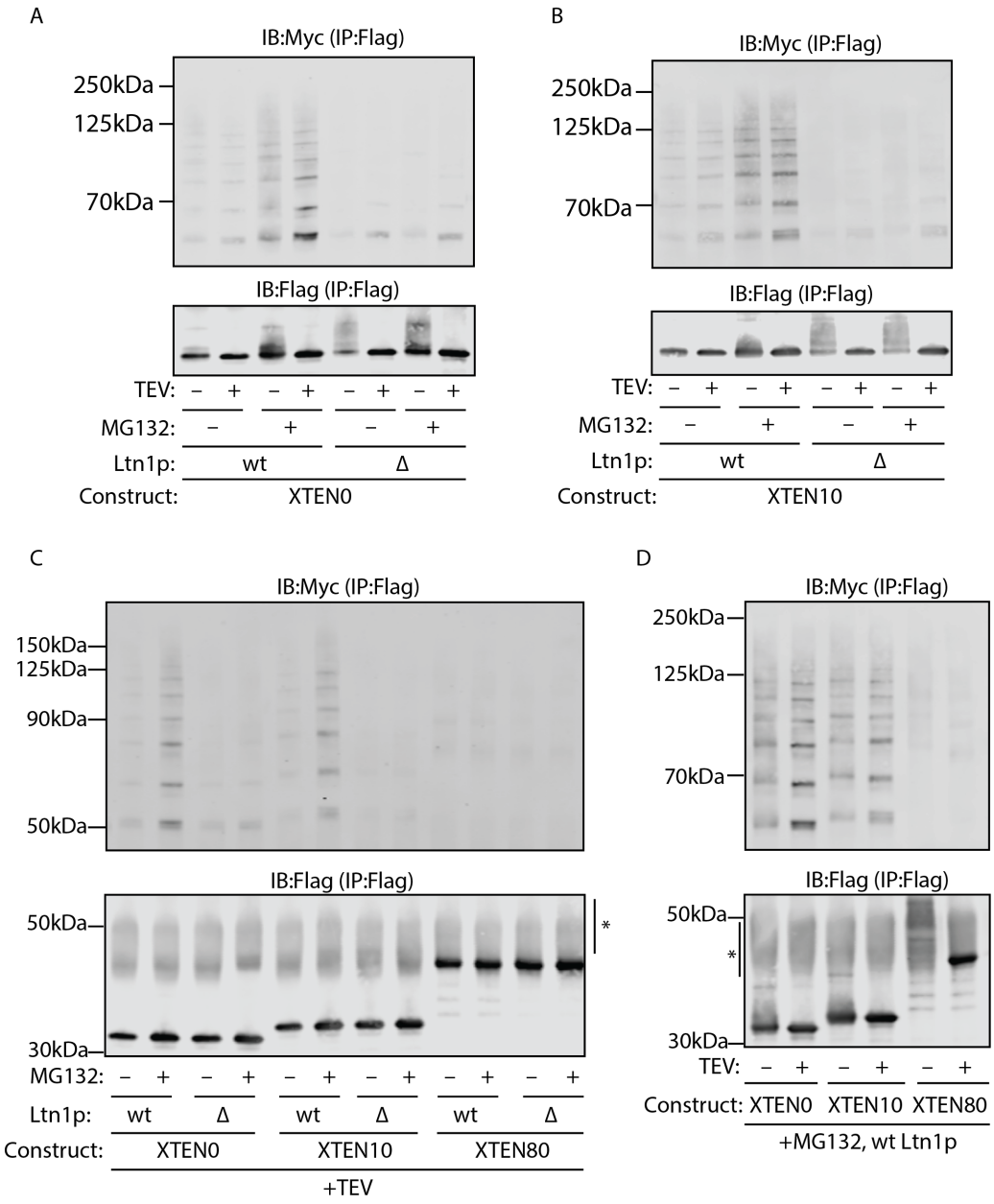

Figure 6. TEV protease digest of ubiquitinated stalling reporters. (**A-D**) XTEN constructs were expressed in *wt* or *ltn1Δ* cells. All cells expressed Myc-tagged ubiquitin and had the multidrug transporter gene *PDR5* deleted. Cells were treated with the proteasome inhibitor MG132 and SDS-boiled lysates were used for Flag IP. The bound material was treated with TEV protease or mock digested and then analyzed by SDS-PAGE and IB. The asterisk (*) points to a non-specific smear, which is likely a product of the buffer conditions used for the TEV digest.

To determine the number of residues that Ltn1p can reach, we generated $GFP_{Lys\text{-}free}$ constructs with a 3xHA tag upstream of only two lysines positioned at different distances from the R12 stalling site (Fig. 7A). These constructs were degraded in a CAT-tail-dependent manner when the lysines were within or near the ribosome exit tunnel, but not when the lysines were 89 amino acids away.

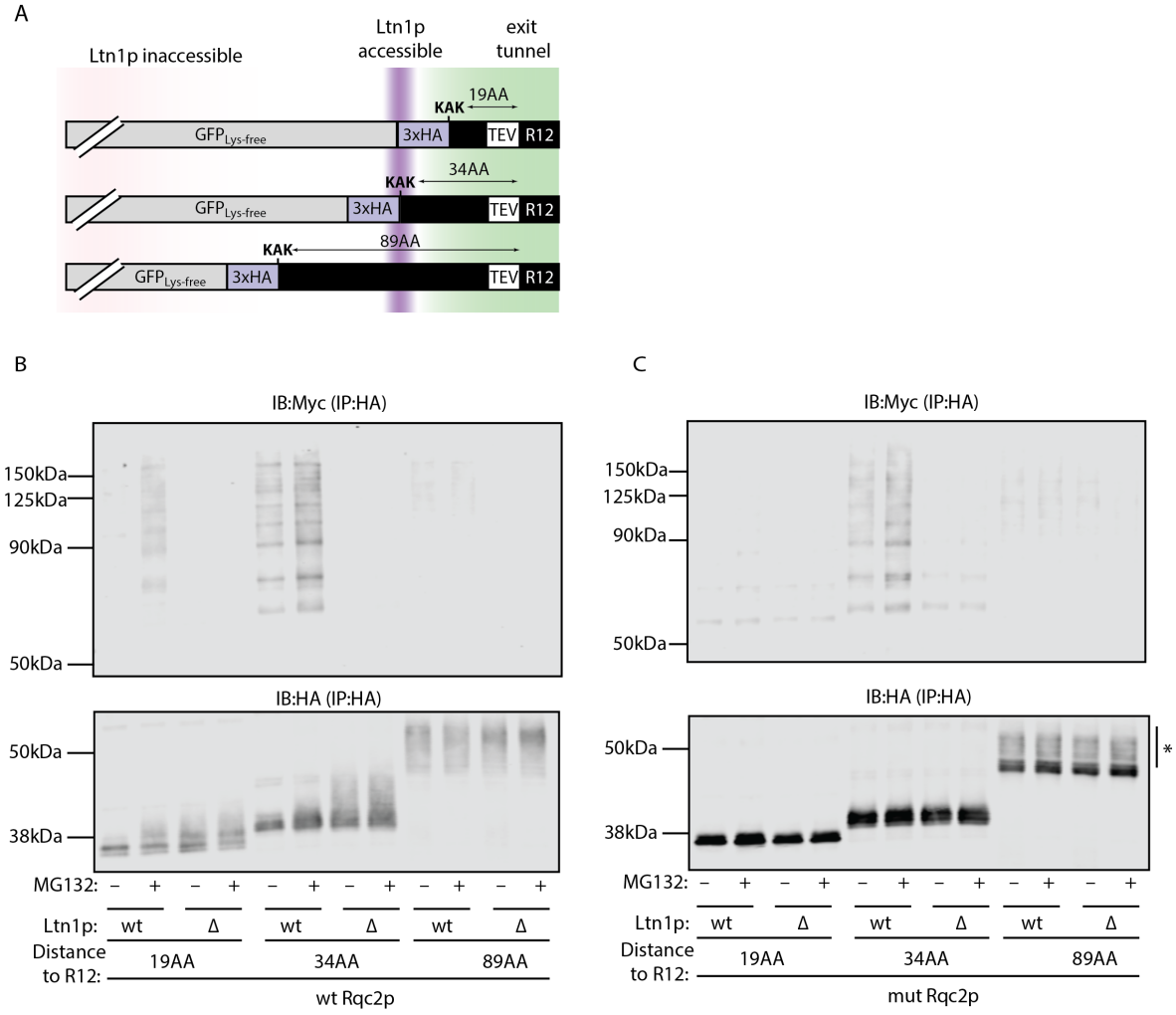

Figure 7. Ubiquitination of stalling constructs is influenced by lysine positioning. (**A**) Schematic of the stalling constructs used for ubiquitin detection. Ribosome exit tunnel (~32 amino acids) and Ltn1p-accessible window (~12 amino acids) are highlighted in green and purple respectively. (**B**, **C**) $GFP_{Lys\text{-}free}$ with two lysines positioned at 19, 34 or 89 amino acids away from the 12R stalling site were expressed in *wt* or *ltn1Δ* cells harboring wild type (wt) or mutant (mut) Rqc2p. All cells expressed Myc-tagged ubiquitin and had the multidrug transporter gene *PDR5* deleted. SDS-boiled lysates were used for HA immunoprecipitation (IP). The eluate was analyzed by SDS-PAGE and IB.

The discrete position of the lysines in these constructs allowed us to refine the Ltn1p accessible window to ~12 amino acids outside the ribosome exit tunnel. As observed with the FLAG-based constructs, the differences in degradation were consistent with differences in Ltn1p-mediated ubiquitination of the substrates (Fig. 7B, C). In line with degradation experiments, wild-type Rqc2p allowed Ltn1p-dependent ubiquitination of the constructs placing lysines 19, and 34 amino acids away from the stall, but not when lysines were 89 amino acids away. In the presence of CAT-tail deficient Rqc2p, only the construct with lysines 34 amino acids from the stall (right outside of the exit tunnel) could be ubiquitinated by Ltn1p (Fig. 7). In fact, only one lysine residue is required for efficient ubiquitination by Ltn1p. This similar construct encodes only one lysine upstream of an HA tag, that remains sequestered in the exit tunnel upon stalling. Although it can be ubiquitinated and degraded with wild-type Rqc2p, mutant Rqc2p cannot use CAT-tails to push this lysine out of the exit tunnel, therefore rendering it resistant to degradation (Fig. 8). Together, we determined the ubiquitin-dependent degradation by RQC requires at least one lysine within the narrow window of accessibility of Ltn1p.

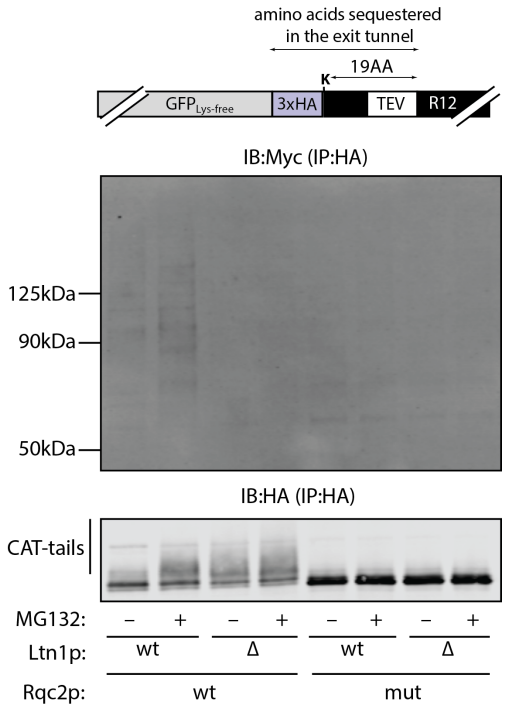

Figure 8. CAT-tailing facilitates Ltn1p-mediated ubiquitination of a single lysine sequestered in the ribosome exit tunnel. $GFP_{Lys\text{-}free}$ with a single lysine sequestered in the ribosome exit tunnel (diagram above) was expressed in *wt*, *ltn1Δ*, $rqc2^{mut}$ or $rqc2^{mut}$/*ltn1Δ* cells. All cells expressed Myc-tagged ubiquitin and had the multidrug transporter gene *PDR5* deleted. SDS-boiled lysates were used for HA IP. The eluate was analyzed on SDS-PAGE and IB.

Upon cross comparison, the Ltn1p accessible window defined using four lysines of the 3xFLAG tag (Fig. 3) was fully consistent with the refined window (Fig. 7) using only two lysines and an HA tag. Thus, the ability of Ltn1p to effectively access residues in a limited window proximal to the exit tunnel is primarily determined by the distance of the lysines from the C-terminus, rather than local sequences or structure.

2.3. CAT-tails expand the number of RQC degradable substrates

Non-stop mRNAs are an important source of natural RQC substrates with lysines sequestered in the exit tunnel (Brandman and Hegde, 2016). For such messages, the ribosome translates the poly(A) tail, which appends AAA-encoded lysines to the C-terminus. The resulting lysines are likely to be sequestered in the ribosome exit tunnel, due to the short length of yeast poly(A) tails (median 27 nucleotides) (Koutmou et al., 2015; Subtelny et al., 2014). Therefore, CAT-tailing can expose lysines that result from translation through the poly(A) tract, allowing efficient ubiquitination and degradation of non-stop decay substrates.

Having established lysine positioning as a critical determinant of CAT-tail-dependent degradation, we next computationally evaluated the frequency with which endogenous substrates would be expected to rely on CAT-tailing for degradation. While the sites of endogenous stalling remain poorly defined, a number of processes such as mRNA fragmentation, oxidative damage (Simms et al., 2014), or stress from translation inhibitors can cause stalling at any position along a message. We therefore considered the nascent chains produced if ribosomes stall with uniform probability at each codon along every coding sequence in the yeast genome (Engel et al., 2014), and we calculated the fraction of potential stalling sites for which there are no lysines accessible to Ltn1p but at least one lysine "hidden" in the ribosome exit tunnel. Based on our experimental estimates of Ltn1p's reach (~12 amino acids) and previous measurements of the length of the ribosome exit tunnel (~35 amino acids) (Ban et al., 2000; Nissen et al., 2000), we estimate that

CAT-tailing substantially increases the fraction of RQC-degradable substrates from ~60% of possible nascent chains to ~95% (Fig. 9).

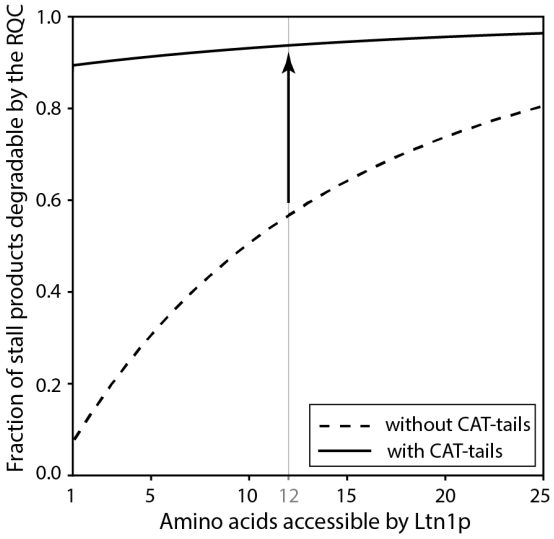

Figure 9. CAT-tail-dependent degradation of endogenous RQC substrates. Fraction of stalling positions leading to an RQC-degradable nascent polypeptide in the presence (solid line) or absence (dashed line) of CAT-tails, graphed as a function of the number of amino acids accessible to Ltn1p and assuming a fixed exit tunnel length of 35 amino acids. The arrow shows the increase in RQC-degradable substrates in the presence of CAT-tails at the estimated Ltn1p reach of 12 amino acids.

Collectively, our studies reveal an unanticipated feature of Ltn1p, the key ubiquitin ligase responsible for RQC-mediated degradation of incomplete nascent chains: Ltn1p is only able to efficiently access lysines that lie within a narrow window of the exit tunnel. This spatial specificity could protect the cell from collateral damage (e.g., degradation of ribosomal proteins or the translocation machinery, as well as unregulated quality control signaling (Higgins et al., 2015; Juszkiewicz and Hegde, 2017)) caused by incidental ubiquitination by Ltn1p. However, the limited reach of Ltn1p presents a challenge to the RQC machinery that must deal with a diverse range of substrates. Without a mechanism to relieve this restriction on lysine positioning, many endogenous RQC substrates would be resistant to Ltn1p-mediated degradation. Our studies

reveal that, in addition to its previously described role in promoting aggregation and inducing a heat shock response (Choe et al., 2016; Defenouillère et al., 2016; Yonashiro et al., 2016b), CAT-tailing acts as a fail-safe mechanism that enables the degradation of a far broader range of substrates by exposing lysines sequestered in the ribosome exit tunnel (Fig. 10).

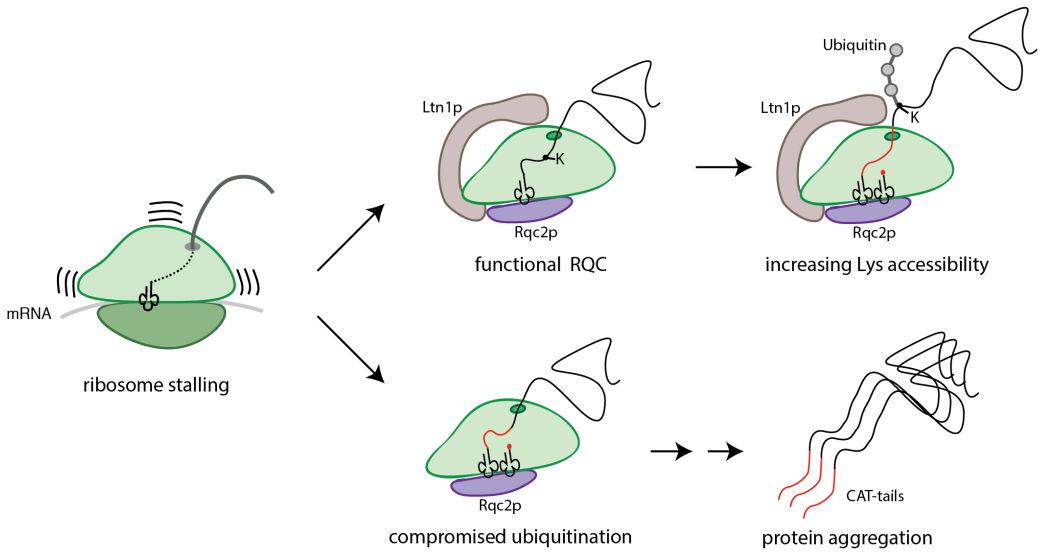

Figure 10. Model for the function of CAT-tails in vivo. CAT-tails lead to aggregation in the presence of a compromised RQC pathway and increase lysine accessibility with an intact RQC complex.

2.4. CRISPRi screen for mammalian factors that promote accumulation of a Non-stop decay substrate

To systematically explore how mammalian cells cope with problematic mRNAs, we designed a mammalian RQC reporter that contains an open-reading frame encoding for the green fluorescent protein, but no stop codon ($GFP_{Non\text{-}stop}$) (Fig. 11A). Since the encoded GFP lacks a stop codon, translation through the GFP to the end of the message causes ribosome stalling and subsequent degradation of the GFP nascent polypeptide via the RQC pathway. Incomplete proteins generated from such messages are model substrates for RQC-mediated degradation in yeast (Bengtson and Joazeiro, 2010) but have not been studied in mammals. Upstream of the GFP, the reporter encodes BFP separated by a T2A ribosome skipping sequence (Fig. 11A). As a result, BFP synthesis is uncoupled from RQC-mediated degradation of GFP, allowing BFP to serve as control for the expression levels of the reporter.

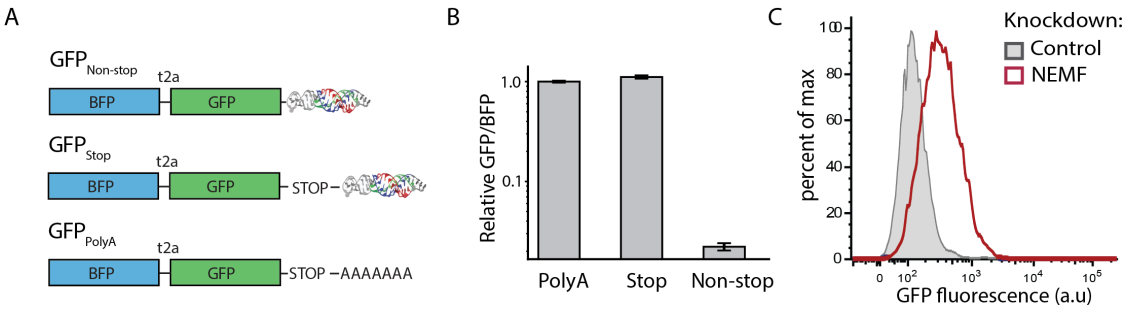

Figure 11. $GFP_{Non\text{-}stop}$ is degraded in an RQC dependent manner. (**A**) Diagrams of non-stop stalling reporter ($GFP_{Non\text{-}stop}$) and control reporters (GFP_{Stop} and GFP_{polyA}) (**B**) Median GFP:BFP ratio of 293T cells transiently transfected with reporter constructs containing the indicated 3' mRNA sequence (median ± SD, N=3). (**C**) GFP fluorescence level in cell lines stably expressing the $GFP_{Non\text{-}stop}$ reporter and control sgRNA or sgRNA against *NEMF*.

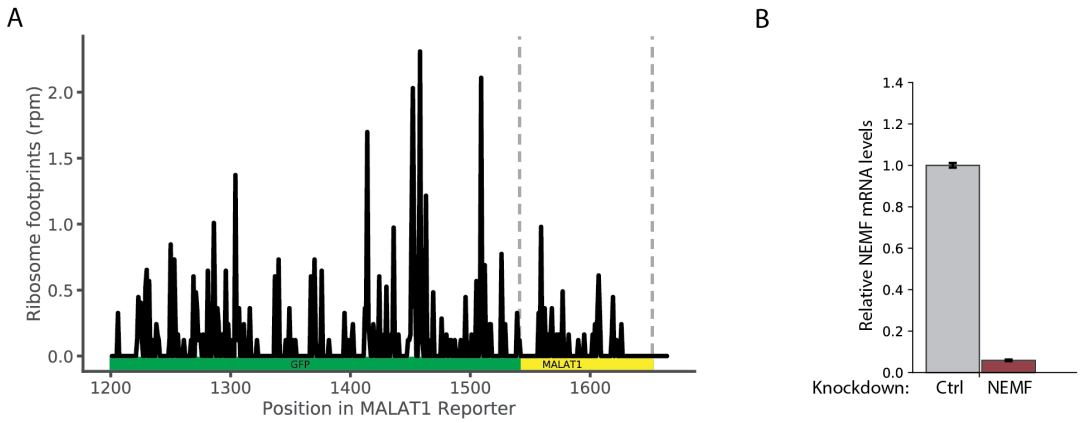

Figure 12. $GFP_{Non\text{-}stop}$ is a non-stop stalling reporter. (**A**) Ribosome occupancy measured by reads per million (RPM) along the $GFP_{Non\text{-}stop}$ reporter. (**B**) Relative *NEMF* mRNA levels measured by qPCR (mean ± SD, N=3).

Since messages lacking a stop codon are rapidly degraded by the exosome (Frischmeyer et al., 2002) we introduced a triple helix derived from the MALAT1 non-coding RNA at the 3' end to stabilize the message (Wilusz et al., 2012). Wild type cells accumulate BFP, but not GFP, resulting in a substantial decrease (~ 100 fold) in the GFP/BFP ratio for the $GFP_{Non\text{-}stop}$ reporter compared to two control reporters that contain either a stop codon before the MALAT1 sequence (GFP_{Stop}), or a stop codon and a canonical polyA tail (GFP_{PolyA}) (Fig. 11A, B, 12A). Knockdown of a core RQC component, *NEMF* (*RQC2* in yeast), led to the stabilization of GFP (Fig. 11C, 12A), confirming the role of mammalian NEMF in degradation of nascent polypeptides resulting from non-stop decay mRNAs (Shao et al., 2015).

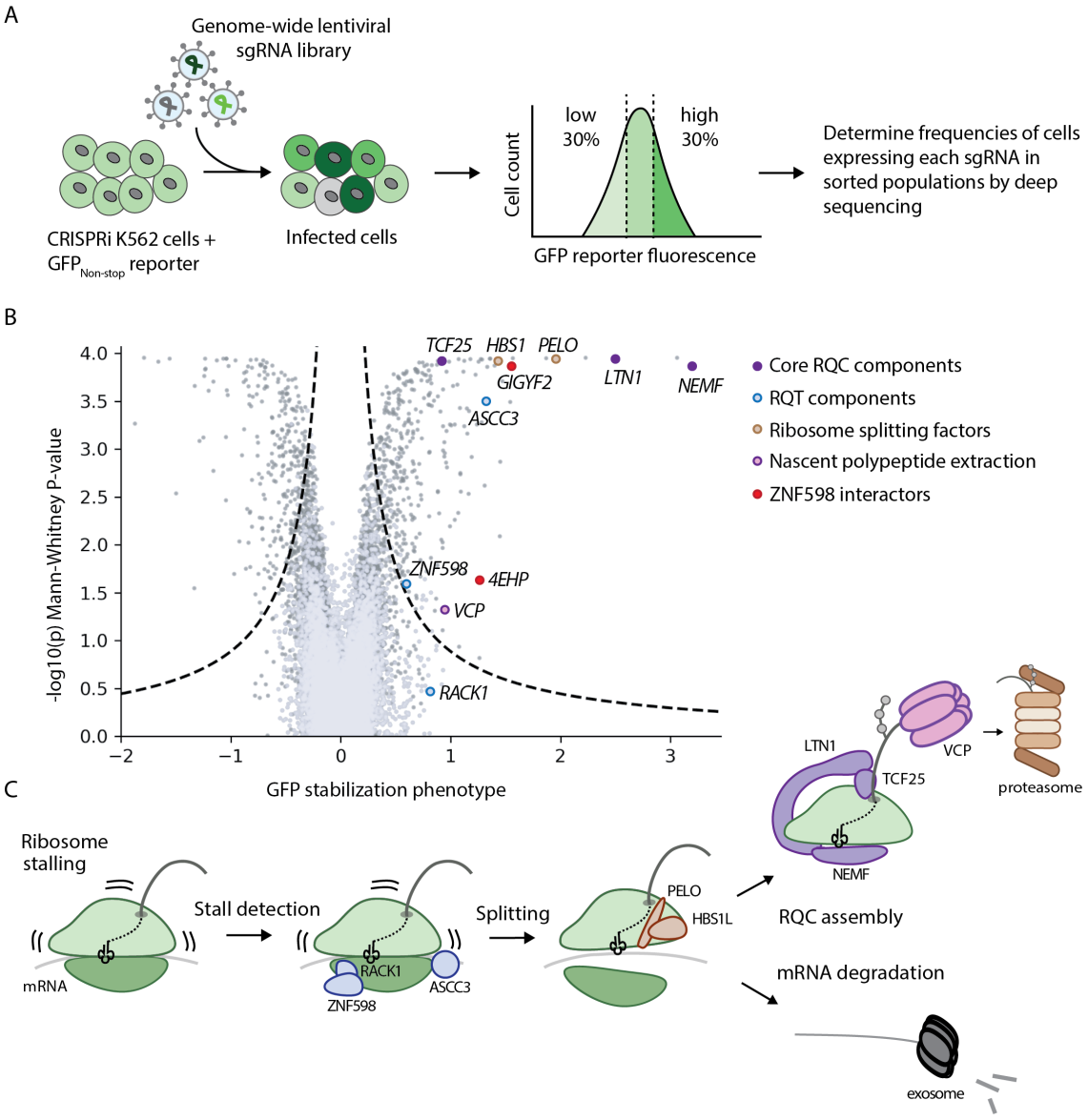

Figure 13. Genome-scale screen for mammalian specific RQC components (**A**) Workflow of FACS-based CRISPRi screen. Reporter cell line constitutively expressing $GFP_{Non\text{-}stop}$ is infected with the whole genome CRISPRi sgRNA library. Knockdown of genes involved in coping with ribosome stalling leads to GFP accumulation. GFP-positive and GFP-negative cells are sorted out and the sgRNAs expressed in those cells are identified via deep sequencing. (**B**) Volcano plot of GFP stabilization phenotype (log_2(GFP high/GFP low) for 3 strongest sgRNAs) and Mann-Whitney P-values from genome-scale CRISPRi FACS screen. Negative controls are shown in lavender, targeting guides in grey, and previously characterized RQC factors are labeled with unique colors. (**C**) Model of the mammalian RQC pathway with screen hits highlighted.

We next used the $GFP_{Non\text{-}stop}$ reporter in a fluorescence-activated cell sorting (FACS)-based genome-wide CRISPRi screen to gain a comprehensive view of mechanisms that cells have for minimizing the accumulation of nascent polypeptides resulting from mRNAs lacking a stop codon. We engineered a K562 mammalian cell line that constitutively expresses the $GFP_{Non\text{-}stop}$ reporter and the dCas9-KRAB CRISPRi effector (Gilbert et al., 2014) and transduced this cell line with an sgRNA library (hCRISPRi-v2) targeting all known protein-coding open reading frames (Horlbeck et al., 2016). We hypothesized that depletion of RQC factors will interfere with the ability of the cells to detect stalled ribosomes and degrade the stalled nascent polypeptide, which will result in GFP stabilization. We then sorted the cells with high and low GFP signal via FACS and identified the genes that were depleted in those cells by deep sequencing the sgRNAs they expressed. (Fig. 13A). The screen identified the majority of known components from each stage of the RQC pathway (stall detection, ribosome splitting, nascent chain extraction, mRNA and peptide degradation) as top hits (Fig. 13B, C, 14A, B). In addition to factors previously implicated in the RQC pathway, the FACS-based screen yielded several genes with no known RQC-related function.

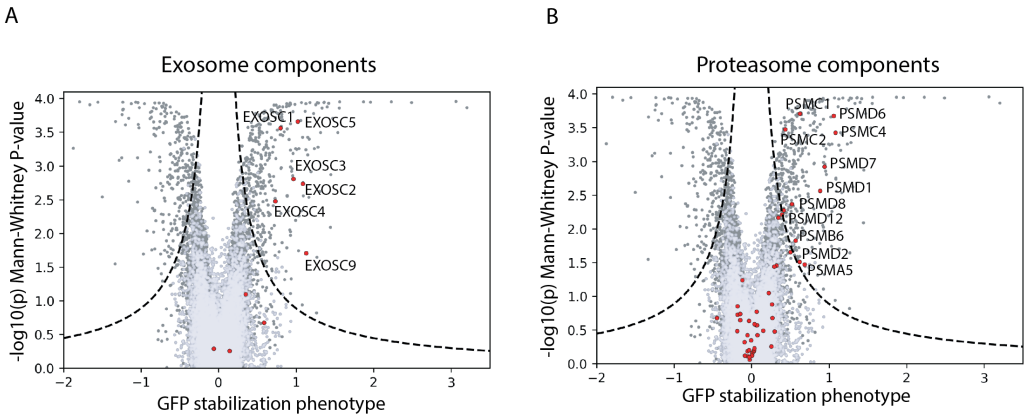

Figure 14. Proteasome and exosome components are hits in GFP screen. (**A, B**) FACS screen volcano plot with exosome or proteasome components highlighted in red.

2.5. Genetic interaction screen identifies the translation inhibitors GIGYF2 and 4EHP as RQC components working in parallel to nascent polypeptide degradation by NEMF

To differentiate between factors that allow mammalian cells to cope with stalled ribosomes as part of the RQC from components of parallel proteostasis pathways, we complemented our reporter-based screen with a growth-based CRISPRi genetic interaction (GI) screen. We aimed to search for components that have synergistic growth defects in combination with loss of NEMF. This idea was motivated in part by recent findings that combined loss of the NEMF homolog in bacteria (RqcH) and the tmRNA/ ssrA pathway, which helps dispose of incomplete translation products, leads to a synergistic growth defect. (Lytvynenko et al., 2019). To test whether similar pathways exist in combination with the mammalian RQC pathway, we took advantage of the growth defect caused by NEMF depletion (Fig. 15A). We engineered a cell line constitutively expressing a *NEMF*-targeting sgRNA, as well as a paired cell line constitutively expressing a non-targeting control sgRNA, and infected both cell lines with the genome-wide CRISPRi sgRNA library (Fig. 15B). We determined the change in the sgRNA abundance over 10 doublings for each cell lines and then compared this change between the two cell lines. We expected that depletion of RQC components will have similar effect on growth alone or in combination with *NEMF* knockdown (buffering interaction) (Fig. 15C). On the other hand, disruption of pathways that work in parallel with RQC to prevent the accumulation of failed translation products is expected to exacerbate the growth phenotype caused by loss of *NEMF* (synergistic interaction). Indeed, the screen revealed several factors that exhibit buffering or synergistic growth interactions with loss of NEMF (Fig. 15D).

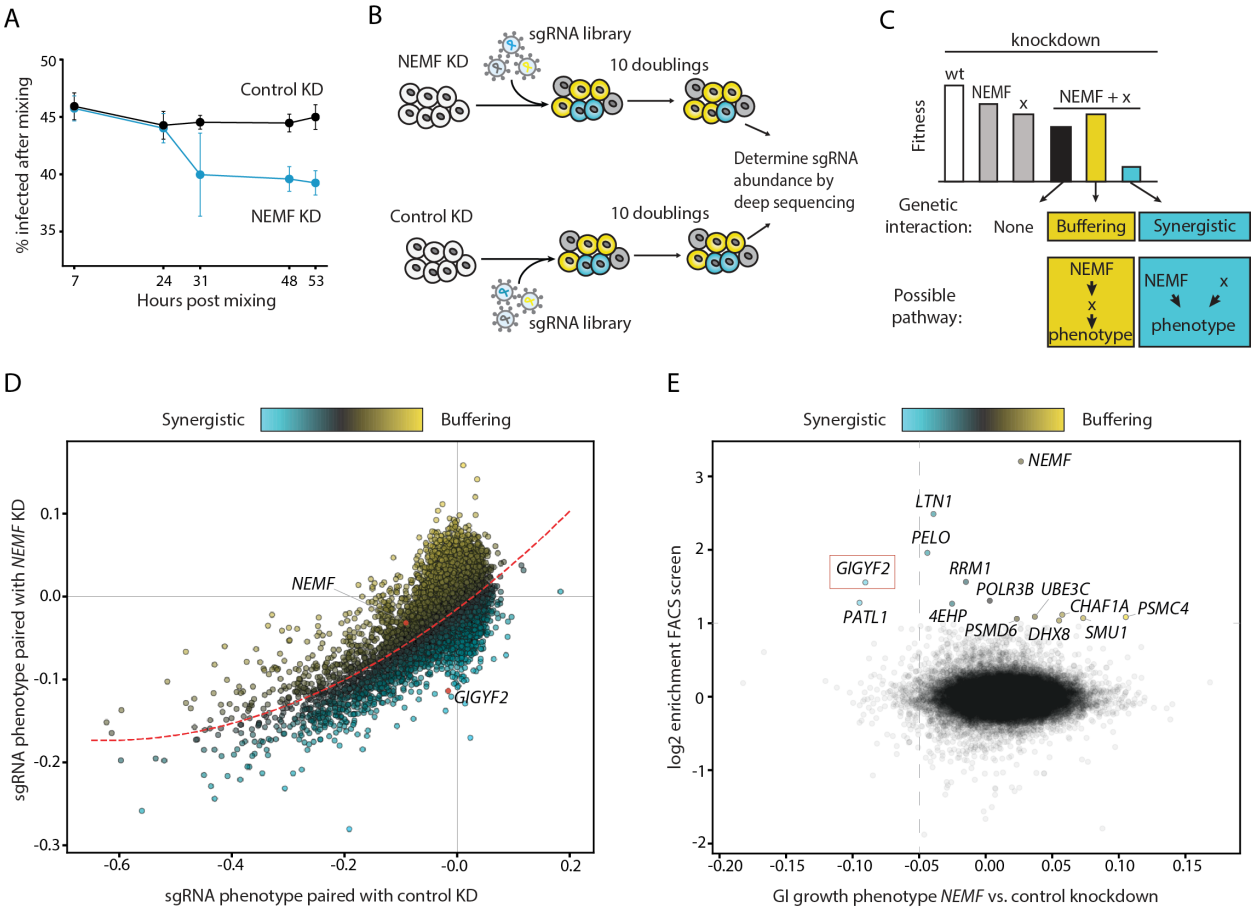

Figure 15. CRISPRi genetic interaction screen for factors that affect the growth of NEMF knockdown cells. (**A**) Competition assay between cells expressing a control or NEMF targeting sgRNA. (B) Workflow of growth-based CRISPRi screen. Control knockdown or NEMF knockdown cell lines were infected with the genome-scale sgRNA library and the change in the sgRNA abundance between the two cell lines following 10 cell doublings was determined by deep sequencing. (**C**) Expected growth phenotypes and predicted biological pathways resulting from knockdown of a hypothetical factor (X) alone or in combination with NEMF. (D) Results from genetic interaction (GI) screen for factors affecting the growth of control or *NEMF* knockdown cells. GI scores were derived by fitting the data to a quadratic curve (red dashed line) and calculating the distance of each point from the best-fit line. Genes exhibiting synergistic interactions with *NEMF* knockdown vs. control knockdown (negative GI score) are marked in blue, and genes with positive GI score (buffering interactions) are in yellow. (**E**) Comparison of FACS and GI CRISPRi screens. Hits from FACS screen (log2 enrichment > 1) that stabilized $GFP_{non\text{-}stop}$ reporter upon individual re-testing are labeled and colored by GI score.

We then compared the hits from the FACS-based reporter screen and the modifier screen. Two genes stood out as having both a strong synergistic interaction with loss of NEMF and stabilizing effect on the RQC reporter upon knockdown: *PATL1* and *GIGYF2* (Fig. 15E). *PATL1* encodes a scaffold protein that bridges mRNA decapping and deadenylation (Ozgur et al., 2010). Stabilization of damaged mRNAs in the absence of PATL1 could explain both the increased levels of stalled nascent polypeptides and the synergistic growth interaction with *NEMF* knockdown, which disposes of incomplete protein products from such damaged mRNAs. We focused our attention on the second gene, *GIGYF2*, which had not been previously implicated in the cellular response to damaged mRNAs.

Overexpression studies of tagged GIGYF2 have shown that it interacts with the inhibitory cap-binding protein 4EHP (Peter et al., 2017) and the ribosome collision sensor ZNF598 (Morita et al., 2012; Tollenaere et al., 2019). Indeed, 4EHP and ZNF598 co-immunoprecipitated with GIGYF2 endogenously tagged with GFP11, confirming that these three proteins interact in cells (Fig. 16A). In addition, GIGYF2 and 4EHP were strongly enriched upon immunoprecipitation of FLAG- tagged ZNF598, as quantified by mass spectrometry (Fig. 17).

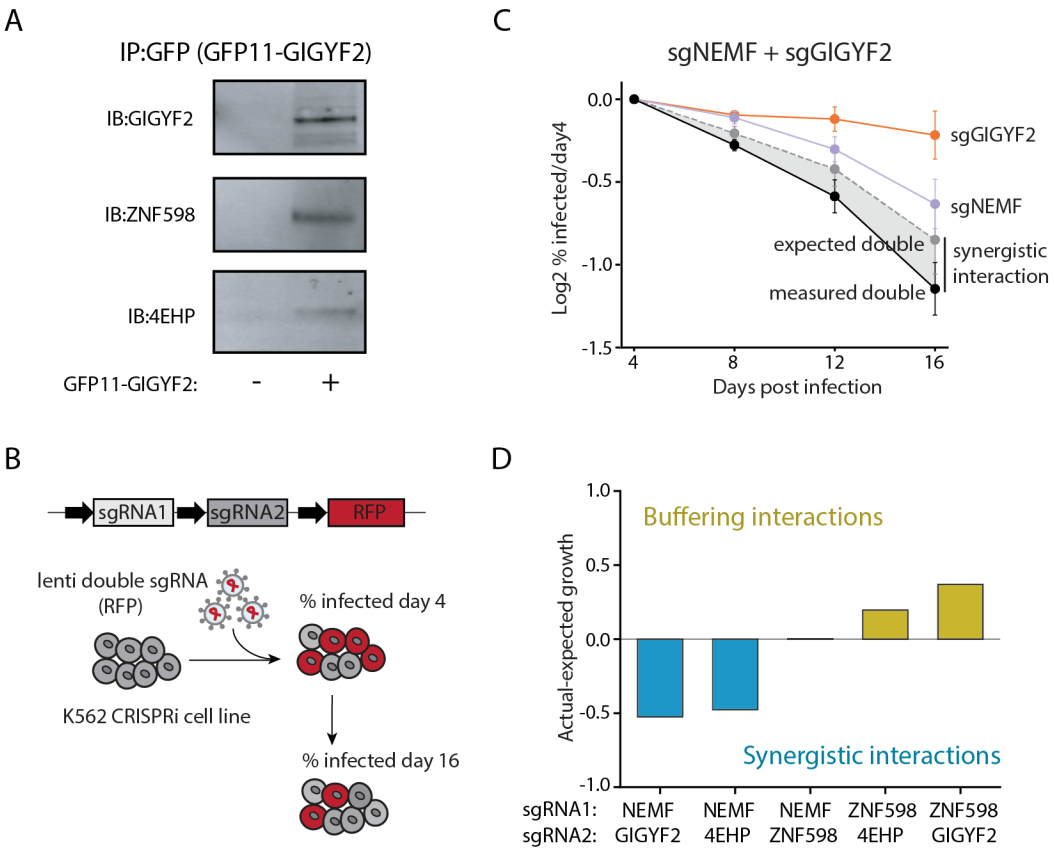

Figure 16. GIGFY2 and 4EHP are components of a pathway parallel to the RQC. (**A**) Immunoprecipitation (IP) and immunoblot (IB) for endogenously tagged GIGYF2, and its binding partners, ZNF598 and 4EHP. (**B**) Outline of growth competition experiments. K562 cells were infected with RFP labeled construct carrying two sgRNAs (targeting + control or two targeting guides). The abundance of RFP positive cells is measured over time via flow cytometry. (**C**) Competition assay among cells expressing sgRNA targeting GIGYF2 and NEMF alone or in combination (mean ± SD, N=2). Dotted grey line highlights the expected growth phenotype and the black line represents the observed growth defect of the double knockdown cells. The deviation from the expected phenotype is indicative of synergistic growth interaction. (**D**) Competition assay of double knockdown cell lines. The bar graph represents the difference in the measured (actual) growth defect and expected phenotype (additive value of single growth defects) on day 16 of the competition assay.

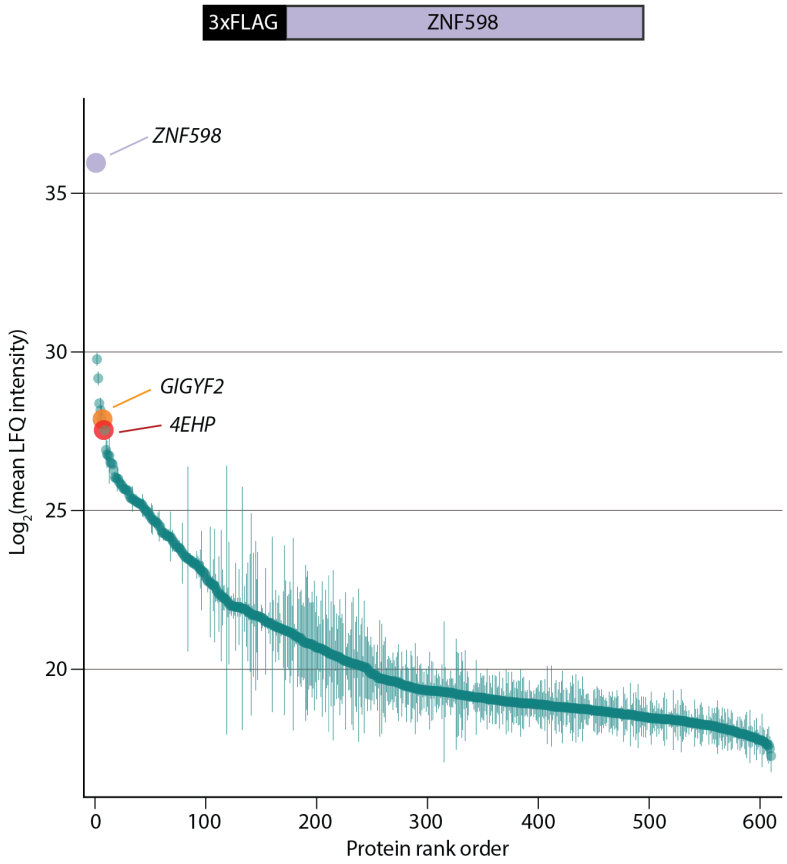

Figure 17. GIGYF2 and 4EHP are top interactors of ZNF598. Ranked proteins identified via mass-spectrometry after 3FLAG-ZNF598 immunoprecipitation (mean ± SD, N=3).

Although an interaction between GIGYF2 and ZNF598 has been reported, the role of GIGYF2 and 4EHP in ribosome-associated quality control has not been explored. Based on our GI screen, knockdown of GIGYF2 or 4EHP in combination with knockdown of NEMF leads to a synergistic growth defect. This result suggests that GIGYF2 and 4EHP function in parallel to the RQC pathway to counter accumulation of toxic polypeptides resulting from ribosome stalling. We were able to recapitulate the GI screen results in targeted studies (Fig. 16B, C). The moderate growth phenotype imparted by knockdown of *NEMF* was exacerbated by *GIGYF2* knockdown (Fig. 16C). Similarly, *4EHP* knockdown also had a synergistic interaction with *NEMF* knockdown, suggesting that GIGYF2 and 4EHP work in parallel to NEMF. In addition,

ZNF598 knockdown had buffering interactions with GIGYF2 and 4EHP (Fig. 16D, 18A, B) consistent with the data that these three proteins form a complex and work together in the same pathway.

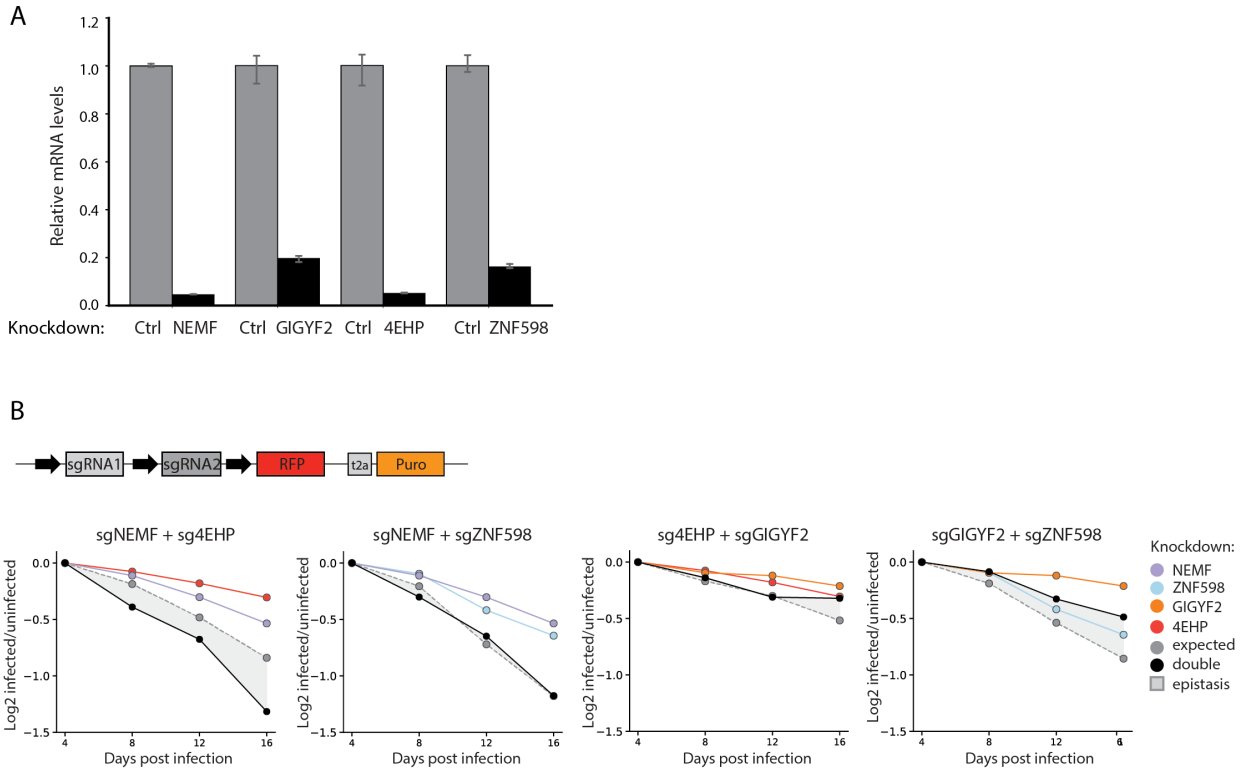

Figure 18. GIGYF2 and 4EHP have a synergistic growth interaction with loss of NEMF. (**A**) Relative mRNA levels for *NEMF, GIGYF2, 4EHP,* and *ZNF598* upon knockdown measured by qPCR (mean ± SD, N=3). (**B**) Competition assays between control cells and cells harboring a single or double knockdown of *NEMF*, ZNF598, *GIGYF2,* and *4EHP.*

2.6. GIGYF2, 4EHP, and ZNF598 inhibit translation of faulty mRNAs

4EHP (EIF4E2) is an ortholog of the mRNA cap-binding and translation initiation factor EIF4E1. However, 4EHP cannot bind EIF4G and as a result it blocks assembly of productive EIF4F initiation complex (Rom et al., 1998; Zuberek et al., 2007), thereby repressing translation of the bound mRNA. Indeed, recruitment of GIGYF2 or 4EHP to reporter messages has been shown to block translation initiation (Kryszke et al., 2016; Morita et al., 2012). It has been hypothesized that GIGYF2 requires an adapter protein for recruitment to its target mRNA, although the endogenous substrates and recruitment factors remain incompletely characterized. Our genetic and biochemical studies suggest a model in which ZNF598 could act as one such factor that recruits GIGYF2 and 4EHP to messages harboring stalled ribosomes, which ultimately leads to translational silencing of the mRNA.

To test this model, we measured the effect of knocking down these proteins on the $GFP_{Non\text{-}stop}$ fluorescent reporter. We compared the levels of BFP, which is released before stalling and is, therefore, a readout of the reporter expression levels, and GFP, which is degraded due to ribosome stalling (Fig. 19A). As expected, knockdown of *NEMF*, a factor involved in the degradation of the stalled nascent polypeptide, increased GFP, but not BFP levels. Knockdown of *GIGYF2* or *4EHP,* however, increased the levels of both fluorescent proteins (Fig. 19A) without affecting reporter mRNA levels (Fig. 19B), or protein half-life (Fig. 20) supporting the hypothesis that these two factors are translation inhibitors.

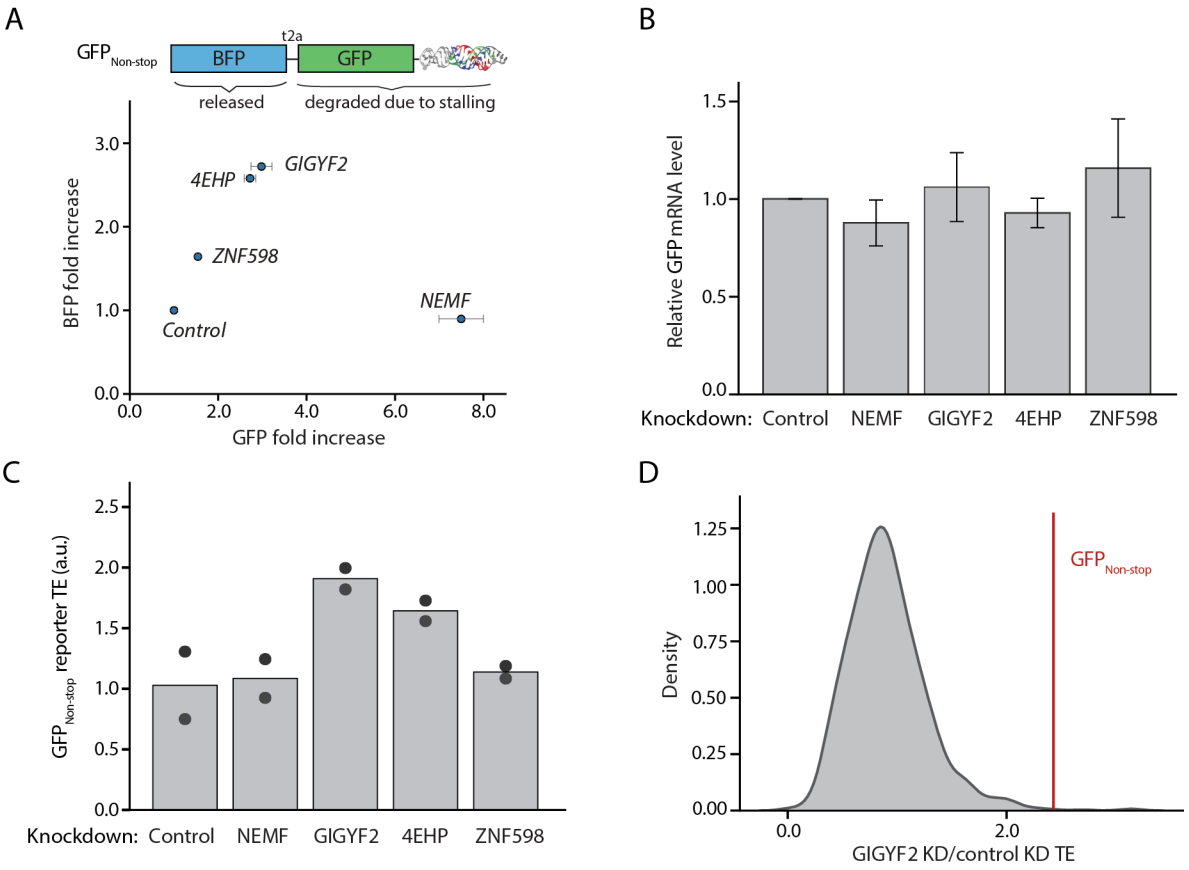

Figure 19. GIGYF2 and 4EHP selectively inhibit translation of faulty messages harboring stalled ribosomes. (A) BFP and GFP fold change upon knockdown of various RQC factors measured by flow cytometry (median ± SD, N=3). **(B)** Relative $GFP_{Non\text{-}stop}$ reporter mRNA levels measured by qPCR upon RQC factors knockdown (mean ± SD, N=3). (**C**) Translation efficiency (TE) of GFP non-stop reporter in knockdown cell (bar plot represents the mean, with data points shown, N=2). (**D**) Histogram of TE change in GIGYF2 knockdown compared to control. $GFP_{Non\text{-}stop}$ reporter is highlighted with a red line.

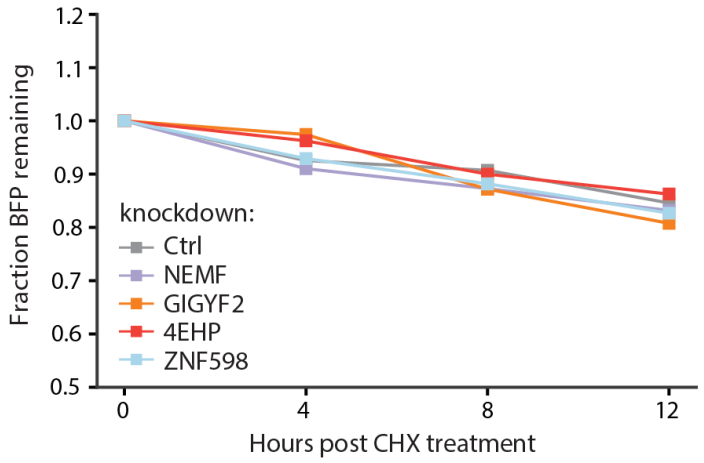

Figure 20. Reporter protein half-life is unaffected by knockdown of RQC factors. BFP fluorescence measured after addition of cycloheximide (100 mg/ul) in various knockdown cell lines.

To directly measure the changes in ribosome occupancy on our $GFP_{Non\text{-}stop}$ stalling reporter, we performed ribosome profiling. Consistent with the fluorescent reporter assay, the translation efficiency (TE) of the reporter was increased in both GIGYF2 and 4EHP knockdown cell lines (Fig. 19C), with minimal changes in the reporter mRNA expression levels (Fig. 21A). When compared to endogenous messages with similar expression levels, the $GFP_{Non\text{-}stop}$ reporter has one of the highest TE changes upon loss of GIGYF2 (Fig. 19D, 21B). In addition, we find that the TE of endogenous messages is not affected by GIGYF2 or 4EHP knockdown, regardless of their expression levels (Fig. 21C, D). Taken together, these data support a model where GIGYF2/4EHP block translation on problematic messages.

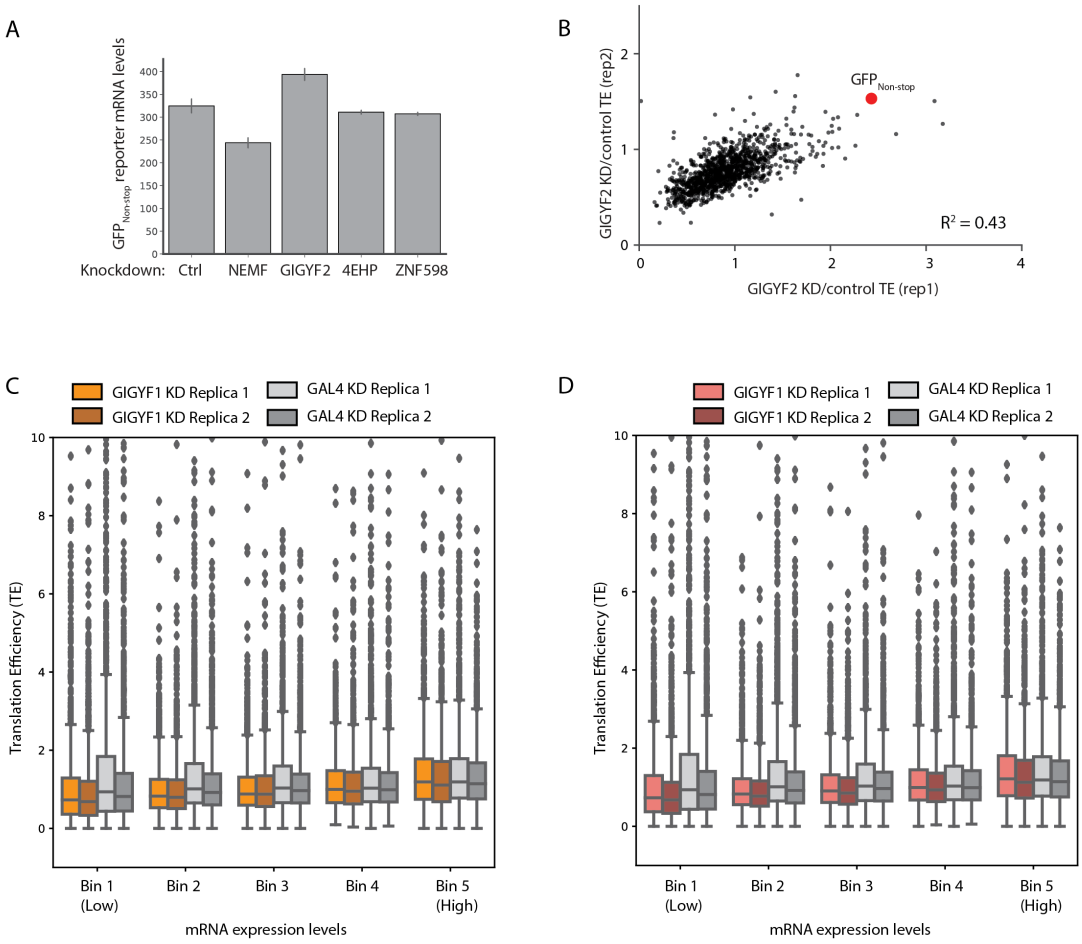

Figure 21. GIGYF2 and 4EHP block translation initiation on faulty mRNAs. (**A**) mRNA levels of $GFP_{Non\text{-}stop}$ reporter in knockdown cell lines. (**B**) Translation efficiency (TE) change for endogenous genes and $GFP_{Non\text{-}stop}$ stalling reporter (red dot) in GIGYF2 knockdown vs. control cells. (**C, D**) TE of endogenous mRNAs binned by mRNA expression level in GIGYF2 or 4EHP knockdown cells.

To ensure that the observed translational effect was specific to faulty mRNAs, and not due to global changes in protein production, we used a second set of reporters with bidirectional promoters. One promoter drives expression of an mRNA coding for GFP with a canonical stop codon and polyA tail, and the other drives a non-stop reporter ($RFP_{Non\text{-}stop}$) or a control fluorescent protein (RFP_{Stop}) on a separate mRNA. Importantly, these cell lines have similar expression levels for the stalling and non-stalling reporters as confirmed by qPCR (Fig. 23A, B).

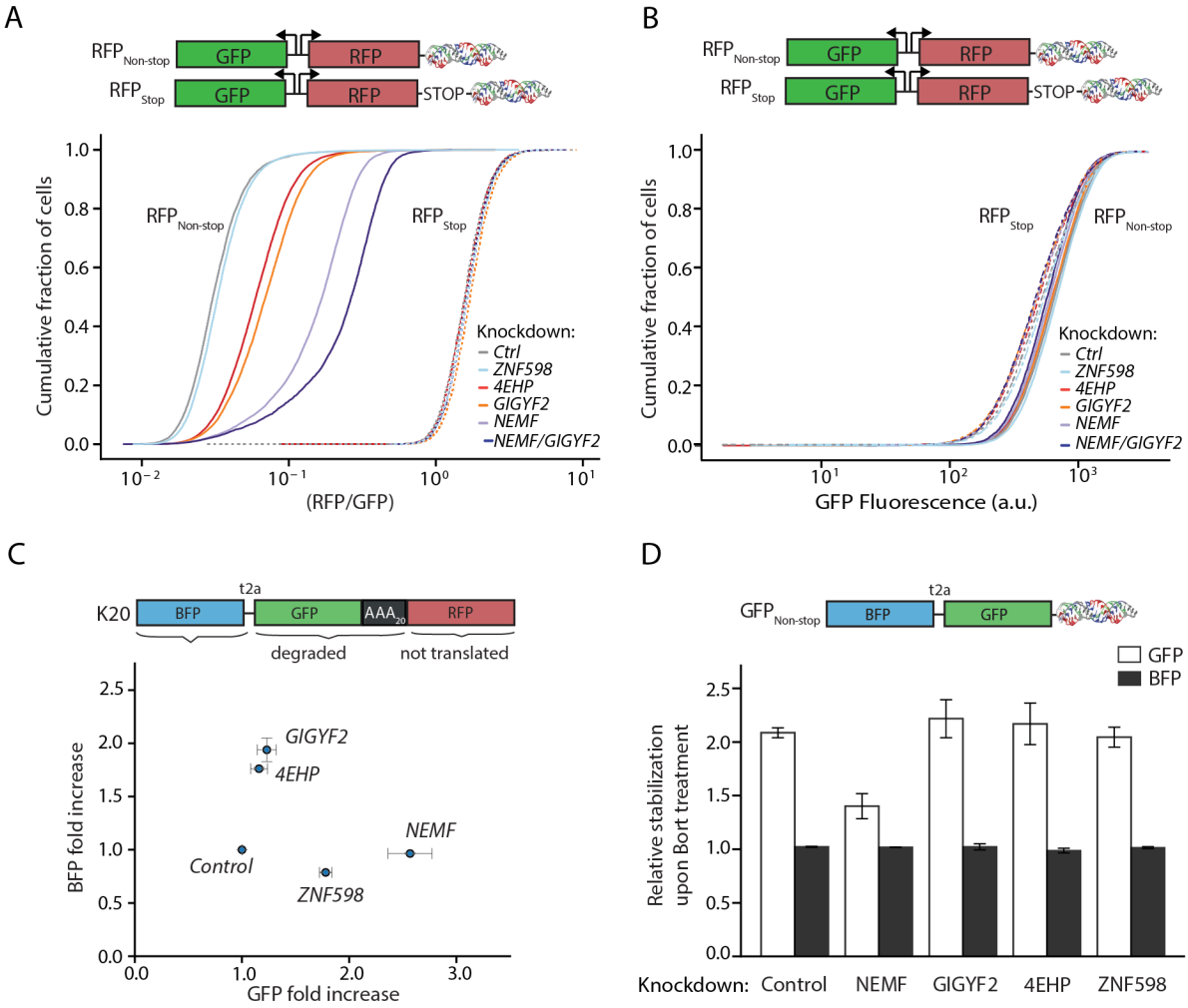

Figure 22. GIGYF2 and 4EHP selectively inhibit translation of multiple faulty messages without global effects on translation. (**A**) Bidirectional promoters were used to express GFP with stop codon and polyA tail, and RFP with or without stop codon (diagramed above). Cumulative distribution plot of RFP/GFP protein ratios measured by flow cytometry in RQC knockdown cells lines. Cells expressing $RFP_{Non\text{-}stop}$ reporters are shown as solid lines, whereas cells harboring RFP_{stop} are shown as dashed lines. (**B**) Cumulative distribution plot of GFP protein levels measured by flow cytometry in RQC knockdown cells lines. Solid and dashed lines represent GFP signal from reporter also containing $RFP_{Non\text{-}stop}$ or RFP_{stop} respectively. (**C**) BFP and GFP protein fold change of K20 stalling reporter upon RQC factors knockdown (median ± SD, N=2). (**D**) Cells expressing $GFP_{Non\text{-}stop}$ reporter were treated with the proteasome inhibitor Bortezomib for 3h and the BFP and GFP protein stabilization was measured by flow cytometry (median ± SD, N=2).

Knockdown of *NEMF*, *GIGYF2*, and *4EHP* increased the RFP/GFP ratio for $RFP_{Non\text{-}stop}$, but not RFP_{Stop} (Fig. 22A). These knockdowns did not have a global effect on translation as the levels of the non-stalling controls were unchanged (Fig. 22B, 23C-F). The observed $RFP_{Non\text{-}stop}$ stabilization was not due to changes in mRNA levels (Fig. 23G), consistent with the $GFP_{Non\text{-}stop}$ reporter used in our original screen. In addition, a simultaneous knockdown of *NEMF* and *GIGYF2* increased the RFP/GFP ratio to a greater extent than either single knockdown, further suggesting that these factors are components of two parallel pathways coping with ribosome stalling.

We confirmed that the observed translational silencing does not depend on the type of stall by measuring the effect of *GIGYF2* and *4EHP* knockdown on a fluorescent reporter containing a previously characterized mammalian stalling sequence, 20 AAA (K20) (Juszkiewicz and Hegde, 2017). Similar to the $GFP_{Non\text{-}stop}$ reporter, knockdown of *GIGYF2* or *4EHP* led to an increase in both GFP and BFP fluorescence levels (Fig. 22C), without a change in mRNA levels (Fig. 23H). In the case of ZNF598, however, knockdown led to the increase of GFP, but not BFP, indicating that the requirement for ZNF598 is specific to the Non-stop substrate, whereas alternative factors may be required to recruit GIGYF2 and 4EHP to No-Go mRNAs. Intriguingly, prior to the discovery of the RQC pathways, it had been suggested that the lack of a stop codon can interfere with translation of a message (Akimitsu et al., 2007). However, the relationship (if any) between that phenomenon, which was believed to act in a post-initiation step resulting in halting of translation before completion of full-length proteins, and the GIGYF2/4EHP-mediated inhibition of translation of Non-stop and No-Go substrates is unclear.

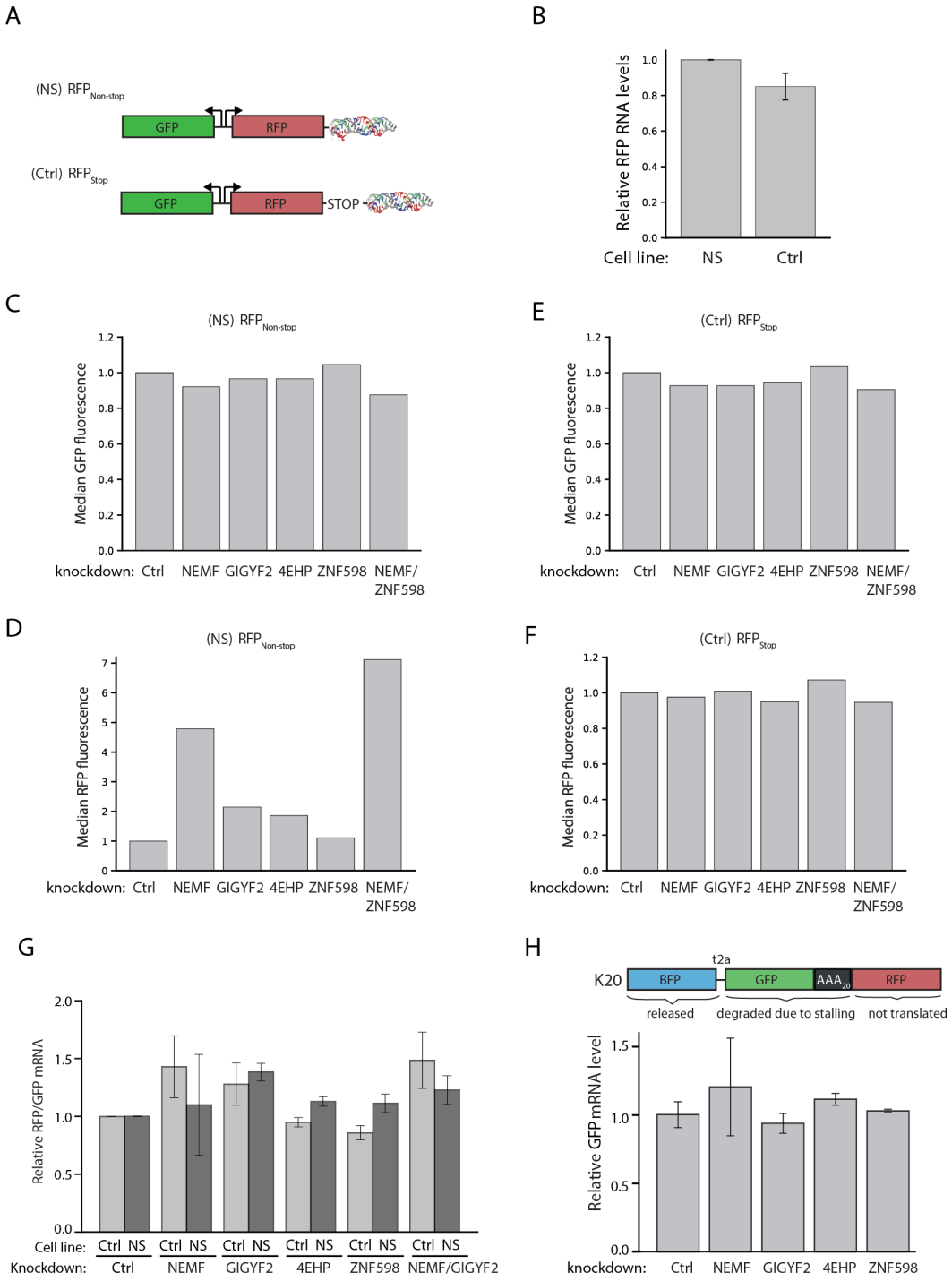

Figure 23. GIGYF2 and 4EHP selectively inhibit translation of faulty mRNAs. (**A**) Diagram of $RFP_{Non\text{-}stop}$ (NS) and RFP_{stop} (Ctrl) bidirectional reporters. (**B**) Relative RFP mRNA levels measured by qPCR (mean ± SD, N=3) from cells stably expressing the NS or Ctrl reporters. (**C-F**) GFP or RFP fluorescence of NS or Ctrl reporter in various knockdown cell lines measured by flow cytometry. (**G**) Relative RFP/GFP mRNA levels in NS or Ctrl reporter cell lines in various knockdown backgrounds measured by qPCR (mean ± SD, N=3). (**H**) Relative GFP mRNA levels for K20 reporter in knockdown cell lines.

Finally, to confirm that GIGYF2 and 4EHP are part of a pathway that works in parallel to RQC-mediated degradation of the stalled nascent polypeptide, we inhibited the proteasome by treating various knockdown cell lines with bortezomib (Fig. 22D). We observed stabilization of the stalled polypeptide in the *GIGYF2, 4EHP* and *ZNF598* knockdown cells lines of the same magnitude as cells expressing a control sgRNA, whereas, knockdown of *NEMF* leads to a much milder increase upon bortezomib treatment, consistent with the role of *NEMF* in UPS-mediated nascent chain degradation. This result indicates that the observed increase in fluorescence upon *GIGYF2* and *4EHP* knockdown is not caused by nascent chain stabilization, but by increased ribosome engagement, and that the partially synthesized polypeptide is still targeted for degradation by RQC.

2.7. The yeast homologs of GIGYF2, Smy2p and Syh1p, destabilize faulty mRNAs

We next explored whether GIGYF2 and/or 4EHP played a role in RQC in yeast. Two potential homologs of GIGYF2 have been identified in yeast, Smy2p and Syh1p (Ash et al., 2010), although they have not been implicated in RQC. To determine if Smy2p and Syh1p play a role in preventing accumulation of incomplete polypeptides, we utilized a previously characterized yeast stalling reporter (D'Orazio et al., 2019). This reporter expresses a no-go substrate and a control fluorescent protein from a bidirectional promoter. The stalling substrate encodes GFP separated by a T2A ribosome skipping sequence from *HIS3* gene containing an internal stretch of non-optimal codons (CGA_{12}). As a control, we used a similar reporter without the CGA12 stalling sequence. We compared the protein levels by flow cytometry and found that knockout of SMY2 and SYH1 alone led to an increase in the GFP/RFP ratio (Fig. 24A). Deleting both homologs led to a greater increase in GFP/RFP compared to the single deletions, suggesting that Smy2p and Syh1p have redundant function. This redundancy could account for the lack of identification of these factors in early RQC screens. Importantly, similar to the human homologs, deletion of the GYF-containing proteins had no effect on global translation. However, in contrast to the mammalian system, the increased expression of the reporter was accompanied by mRNA stabilization of the stalling mRNA, but not control mRNA (Fig. 24B). This observation is consistent with the apparent lack of a 4EHP homolog in yeast, which is an essential part of the mechanism of translation inhibition in mammals. Indeed, the yeast GIGYF2 homologs lack the 4EHP binding domain found in human GIGYF2 (Fig. 24C). However, Smy2p has been shown to bind Eap1p, a protein implicated in mRNA decapping and degradation (Ash et al., 2010). These data suggest that the role GIGYF2-like proteins play in RQC preceded the last common ancestor

of yeast and mammals. Recruitment of GIGYF2 leads to translational silencing in higher eukaryotes, whereas Smy2p and Syh1p mediate RNA decay in yeast.

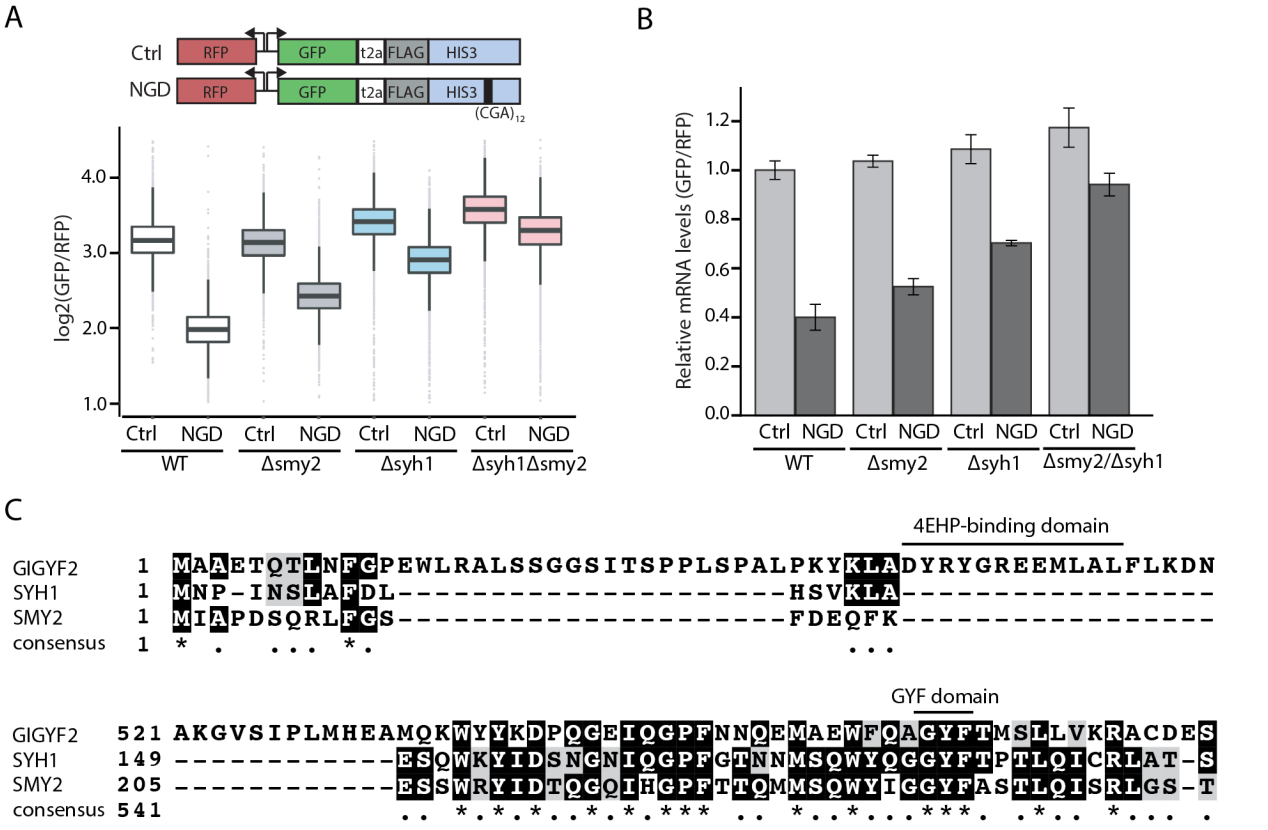

Figure 24. The yeast homologs of GIGYF2, Smy2p and Syh1p, are RQC factors. (A) Schematic of control (ctr) reporter and no-go decay (NGD) reporter containing a stretch of 12 non-optimal CGA codons in the middle of the *HIS3* open reading frame (top). Box plot of GFP/RFP ratios for NGD or control reporter levels in knockout yeast strains measured by flow cytometry (bottom). (**B**) Relative mRNA levels for ctr or NGD reporter in wild type or knockout strains measured by qPCR (mean ± SD, N=3). (**C**) Alignment of regions of GIGYF2, Syh1p, and Smy2p highlighting the 4EHP-binding and GYF domains.

2.8. Recruitment of GIGYF2, 4EHP and ZNF598 leads to translation inhibition

Our genetic and biochemical data suggest that mammalian GIGYF2 and 4EHP can be recruited to problematic messages by the ubiquitin ligase ZNF598 (Juszkiewicz and Hegde, 2017; Sundaramoorthy et al., 2017). To explore this hypothesis, we used an MS2-based system to tether ZNF598, GIGYF2, or 4EHP to a reporter mRNA (Bertrand et al., 1998) (Fig. 25A). We transiently co-expressed a non-stalling reporter ($GFP_{MS2\text{-}stop}$) harboring three MS2 stem-loops in its 5' UTR together with MS2 binding protein (MS2BP) fusions in HEK293T cells. Consistent with published data, recruitment of GIGYF2 or 4EHP to the reporter led to inhibition of translation (Kryszke et al., 2016), as evidenced by a robust decrease in GFP fluorescence without significant changes in the mRNA levels (Fig. 25B, C, 26A). The translation level was not strongly inhibited by MS2BP recruitment alone (Fig. 25B), or overexpression of a FLAG-tagged GIGYF2 protein that does not get recruited to the reporter (Fig. 26B, C), indicating that the observed translational silencing was specific for the tethering of the factors to the mRNA. Additionally, recruitment of ZNF598 to the reporter induced similar translational silencing.

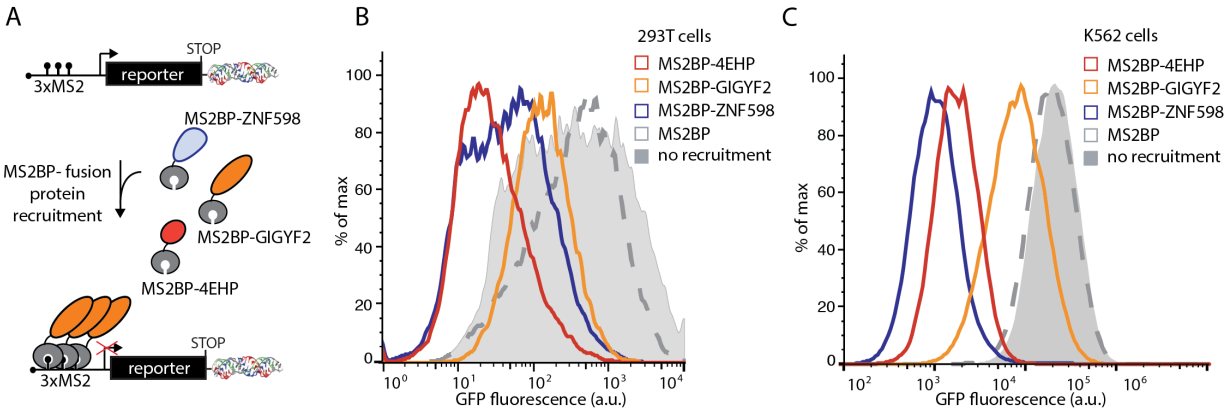

Figure 25. Recruitment of ZNF598, GIGYF2 and 4EHP inhibit translation. (**A**) Schematic of MS2-mediated recruitment of putative silencing factors to a fluorescent reporter. (**B**) GFP fluorescence of $GFP_{MS2\text{-}stop}$ reporter transiently expressed in HEK293T cells alone or with MS2BP-fusion proteins. (**C**) GFP fluorescence of K562 cells stably expressing $GFP_{MS2\text{-}stop}$ reporter alone or in combination with MS2BP-fusion proteins.

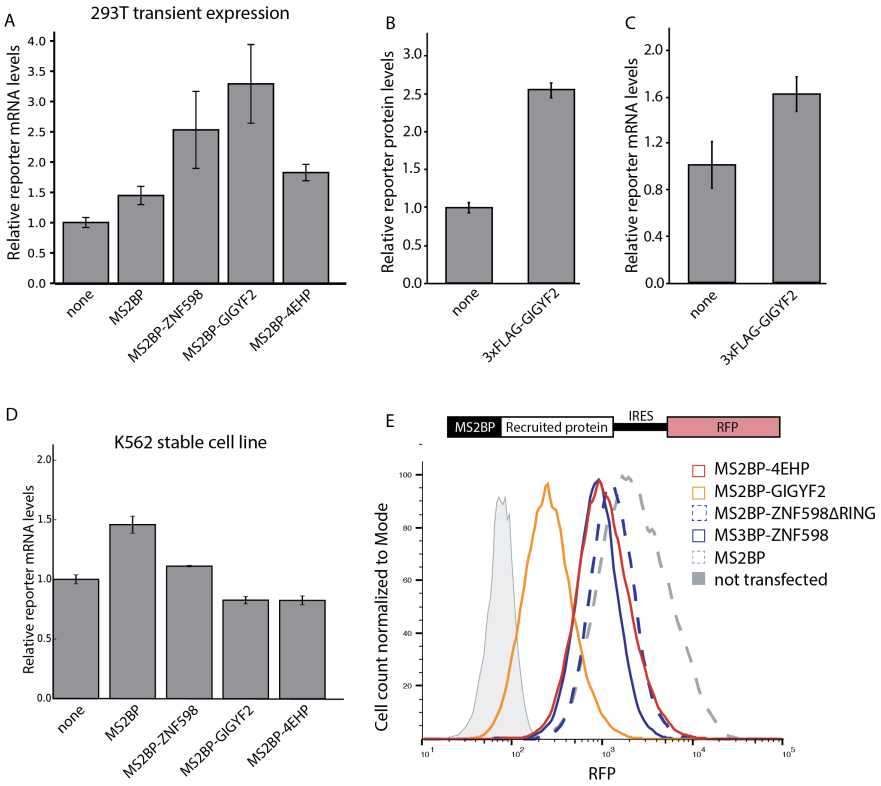

Figure 26. GIGYF2, 4EHP, and ZNF598 inhibit translation when directly recruited to an mRNA. (**A, D**) Relative mRNA levels of $GFP_{MS2\text{-}Stop}$ reporter upon transient or stable expression of MS2BP-fusion proteins measured by qPCR (mean ± SD, N=3). (**B, C**) Protein and mRNA levels of $GFP_{MS2\text{-}Stop}$ measured by flow cytometry or qPCR upon transient expression of 3xFLAG-GIGYF2, that is not directly recruited to the reporter (mean ± SD, N=3). (**E**) MS2BP-fusion proteins expression levels upon stable integration in K562 dCas9-KRAB cells measured by RFP fluorescence.

2.9. Translational inhibition by ZNF598 is mediated by GIGYF2 and 4EHP in a ubiquitination- independent manner

To explore the genetic requirements for translation inhibition, we generated stable cell lines expressing an MS2-fusion protein, as well as $GFP_{MS2\text{-}stop}$ reporter, and CRISPRi machinery (Fig. 25C, 26D). We used CRISPRi to knock down *ZNF598*, *GIGYF2*, or *4EHP* and measured the effect of the knockdown on GFP levels via flow cytometry. Knockdown of *GIGYF2* or *4EHP* alleviated the decrease in GFP fluorescence caused by MS2-ZNF598 (Fig. 27A, 28A-H). Lower expression of the MS2BP-GIGYF2 fusion protein in K562 cells resulted in an attenuated repression phenotype compared to HEK293T (Fig. 26E). Nonetheless, the GIGYF2-mediated repression depended on 4EHP. Similarly, 4EHP-mediated repression depended on GIGYF2, suggesting that these two factors act together to mediate translation inhibition (Fig. 27A). In marked contrast, silencing by neither GIGYF2, nor by 4EHP was impacted by knockdown of *ZNF598* when these factors were directly recruited to the mRNA, indicating that GIGYF2 and 4EHP work downstream and independently of ZNF598. These epistasis experiments support a model in which ZNF598 serves as a scaffold that can recruit GIGYF2 and 4EHP to faulty mRNAs (Fig. 27B).

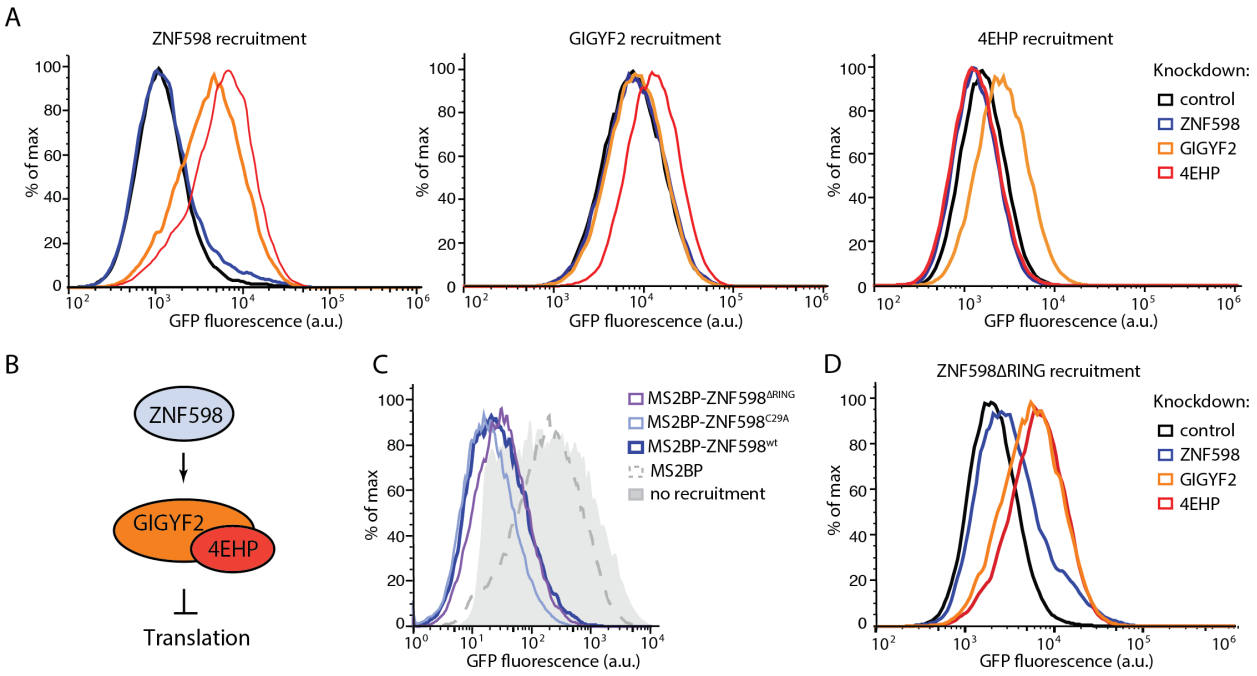

Figure 27. Translational inhibition by ZNF598 is mediated through GIGYF2 and 4EHP in a ubiquitination-independent manner. (**A, D**) MS2-fusion protein is recruited to the $GFP_{MS2\text{-}stop}$ reporter in control cells or knockdown cells for ZNF598, GIGYF2 or 4EHP. The effect of the knockdown on the ability of the fusion protein to silence translation from the reporter is measured via the change in GFP fluorescence. (**B**) Model for GIGYF2 and 4EHP recruitment to mRNA by ZNF598. (**C**) GFP fluorescence from $GFP_{MS2\text{-}stop}$ reporter upon MS2-mediated recruitment of wild type or ubiquitination incompetent ZNF598 ($ZNF598^{C29A}$ or $ZNF598^{\Delta RING}$).

ZNF598 recognizes collided stalled ribosomes and ubiquitinates the small subunit of the ribosome, which triggers ribosome splitting and subsequent RQC complex engagement (Ikeuchi et al., 2019; Juszkiewicz et al., 2018). We next tested whether ZNF598-mediated ubiquitination is required for translational repression by GIGYF2 and 4EHP. We generated ubiquitination-deficient MS2BP-ZNF598 fusion proteins that harbored inactivating mutations in the RING domain (C29A) or deletions of the entire domain (ΔRING) (Sundaramoorthy et al., 2017) and compared their ability to translationally silence the $GFP_{MS2\text{-}stop}$ reporter. Surprisingly, both

mutants were capable of repressing translation (Fig. 27C, 29A). Recruitment of a stably integrated MS2BP-ZNF598ΔRING also repressed translation in a GIGYF2 and 4EHP-dependent manner matching the recruitment of wild-type ZNF598. (Fig. 27D, 29B). These data suggest that ZNF598 has a dual function when it engages collided ribosomes. It serves as a ubiquitin ligase that mono-ubiquitinates the 40S small subunit, triggering release of the stalled ribosome and subsequent RQC engagement, and nascent polypeptide degradation (Juszkiewicz et al., 2018; Sundaramoorthy et al., 2017). In addition, ZNF598 also serves as a scaffold that provides one mechanism for the recruitment of GIGYF2 and 4EHP to the mRNA, in a ubiquitination-independent manner. Once recruited, GIGYF2 and 4EHP sequester the mRNA cap, blocking ribosome initiation and decreasing the translational load on problematic messages.

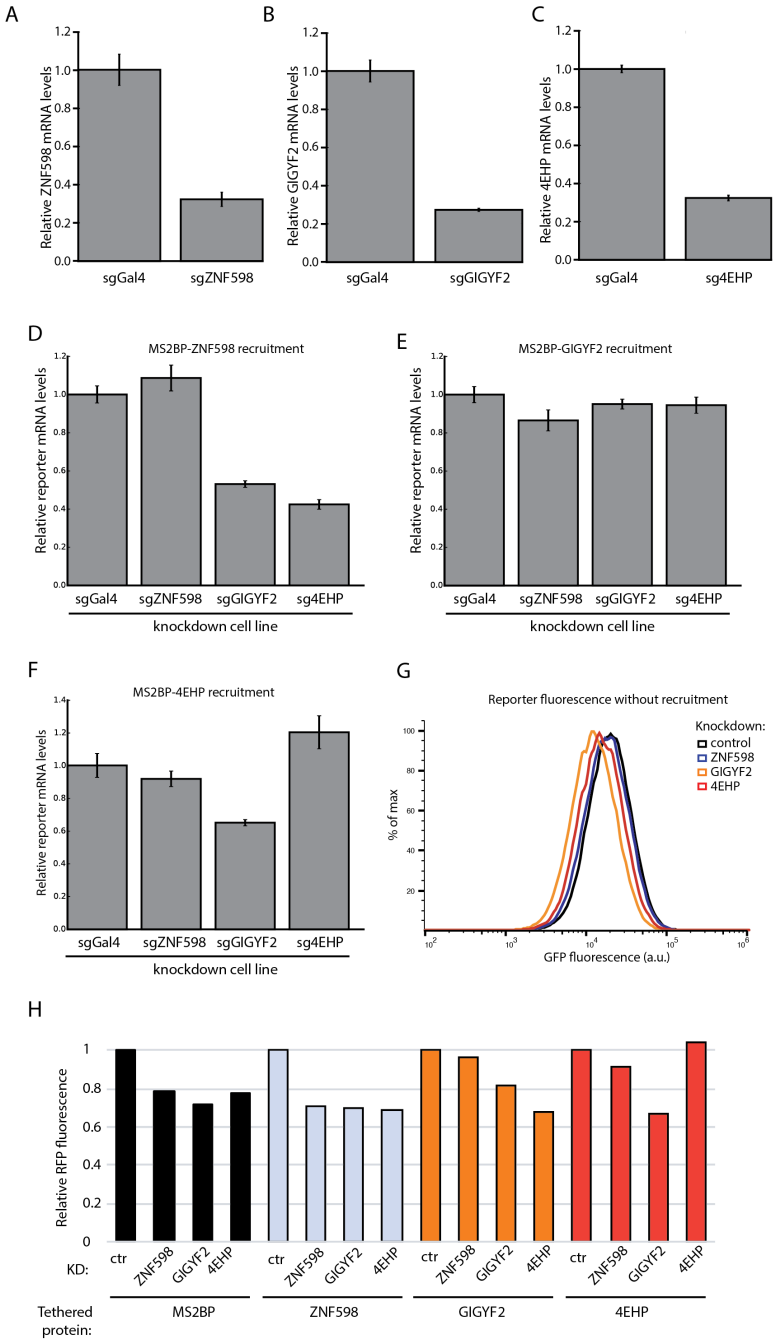

Figure 28. ZNF598 mediated translation inhibition requires GIGYF2 and 4EHP. (**A - C**) Relative mRNA levels upon control (Gal4) or targeting (ZNF598, GIGYF2, 4EHP) knockdown in cells stably expressing $GFP_{MS2\text{-}Stop}$ reporter (mean ± SD, N=3). (**D - F**) Relative $GFP_{MS2\text{-}Stop}$ reporter mRNA levels in knockdown cell lines upon MS2-fusion protein recruitment (mean ± SD, N=3). (**G**) $GFP_{MS2\text{-}Stop}$ reporter proteins expression levels measured by GFP fluorescence upon control, GIGYF2, 4EHP, or ZNF598 knockdown. (**H**) Relative MS2BP-fusion proteins expression levels measured by RFP fluorescence upon control, GIGYF2, 4EHP, or ZNF598 knockdown.

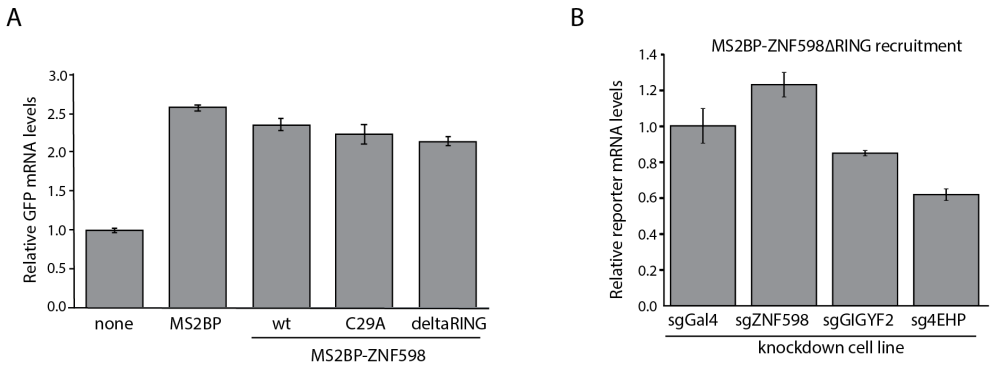

Figure 29. ZNF598 mediated translation inhibition is ubiquitination independent. (**A**) Relative mRNA levels of $GFP_{MS2\text{-}Stop}$ reporter upon MS2BP-ZNF598 (wt, C29A, ΔRING) recruitment (mean ± SD, N=3). (**B**) Relative mRNA levels of $GFP_{MS2\text{-}Stop}$ reporter in knockdown cell lines upon MS2BP-ZNF598 (wt and ΔRING) fusion protein recruitment (mean ± SD, N=3).

2.10. GIGYF2 and 4EHP can be recruited to faulty mRNAs in a ZNF598-independent manner.

The translation phenotype of *ZNF598* knockdown is consistently weaker than that seen with *GIGYF2* knockdown alone for Non-stop substrates (Fig. 30A) and ZNF598, unlike GIGYF2, does not have a translational effect on our No-go reporter (Fig. 22C). Moreover, when *GIGYF2* is knocked down, additional depletion of *ZNF598* has no effect on the increased translation of the $GFP_{Non\text{-}stop}$ reporter (Fig. 30A, 32A). This phenomenon is recapitulated by the artificial tethering experiments using MS2; ZNF598 relies on GIGYF2 or 4EHP for translation repression, but GIGYF2 and 4EHP do not require ZNF598 for translational repression when directly recruited to the message.

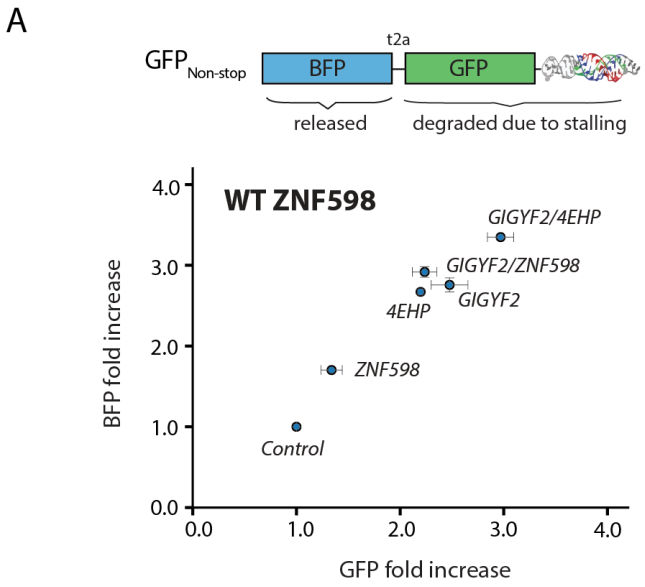

Figure 30. GIGYF2 does not depend on ZNF598 for translation repression. (**A**) BFP and GFP fold change upon single or double RQC factors knockdown measured by flow cytometry (median ± SD, N=2).

These observations can be explained by the presence of alternative recruitment mechanisms for GIGYF2 and 4EHP to faulty mRNAs, or by technical limitations, such as incomplete *ZNF598* knockdown. Although we achieved over 95% knockdown of *ZNF598* via CRISPRi (Fig. 31B, 32B), we could not exclude the possibility that the remaining ZNF598 is responsible for the observed partial phenotype.

To differentiate between these two hypotheses, we engineered a *ZNF598* knockout cell line using CRISPR/Cas9 and confirmed that these cells are true knockouts both by western blotting (Fig. 31B, 32B) and sequencing of the genomic locus (Canaj et al., 2019). We integrated the $GFP_{Non\text{-}stop}$ reporter in these cells and measured the effect of *GIGYF2* and *4EHP* knockdown on the GFP and BFP levels.

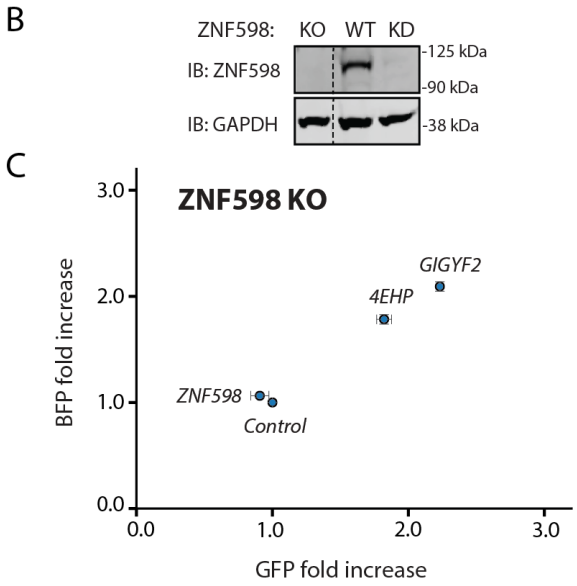

Figure 31. ZNF598-dependent and independent pathways for GIGYF2-4EHP recruitment and RQC. (**B**) Immunoblot (IB) of ZNF598 in wildtype, ZNF598 knockdown, and ZNF598 knockout cell lines. (**C**) BFP and GFP fold change upon RQC factors knockdown in a ZNF598 knockout cell line measured by flow cytometry (median ± SD, N=2).

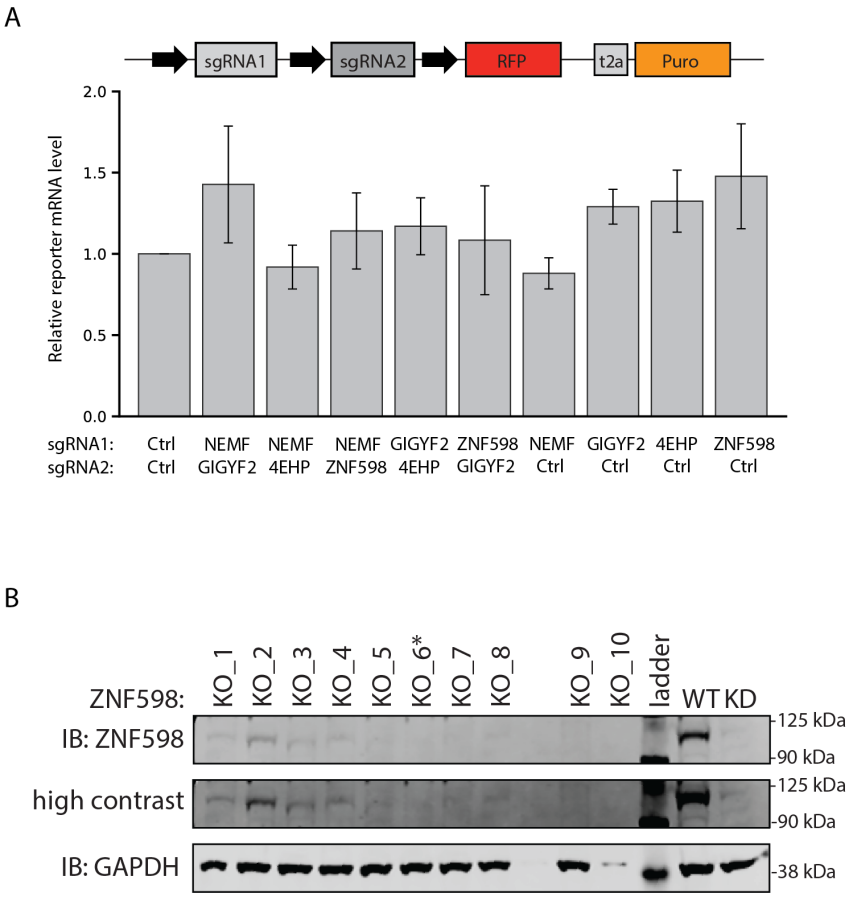

Figure 32. GIGYF2 and 4EHP can be recruited to damaged messages in a ZNF598-independent manner. (**A**) Schematic of double knockdown vector (top). Relative mRNA levels of $GFP_{Non\text{-}stop}$ reporter upon single or double knockdown (mean ± SD, N=3). (**B**) Western blot of ZNF598 knockout clones, as well as cell expressing endogenous wild type ZNF598 (WT) or ZNF598 knockdown cells (KD). GAPDH is used as a loading control. KO_6* was selected for further experiments.

Knocking down these factors led to an increase in both the GFP and BFP fluorescent signals, even though no ZNF598 is present in these cells (Fig. 31C). Importantly, knockdown of *ZNF598* in the knockout cells had no effect on the stalling reporter, confirming the specificity of the CRISPR knockdown. This experiment supports the existence of ZNF598-independent recruitment mechanism(s) that enable GIGYF2 and 4EHP to inhibit translation of damaged messages (Fig. 33)

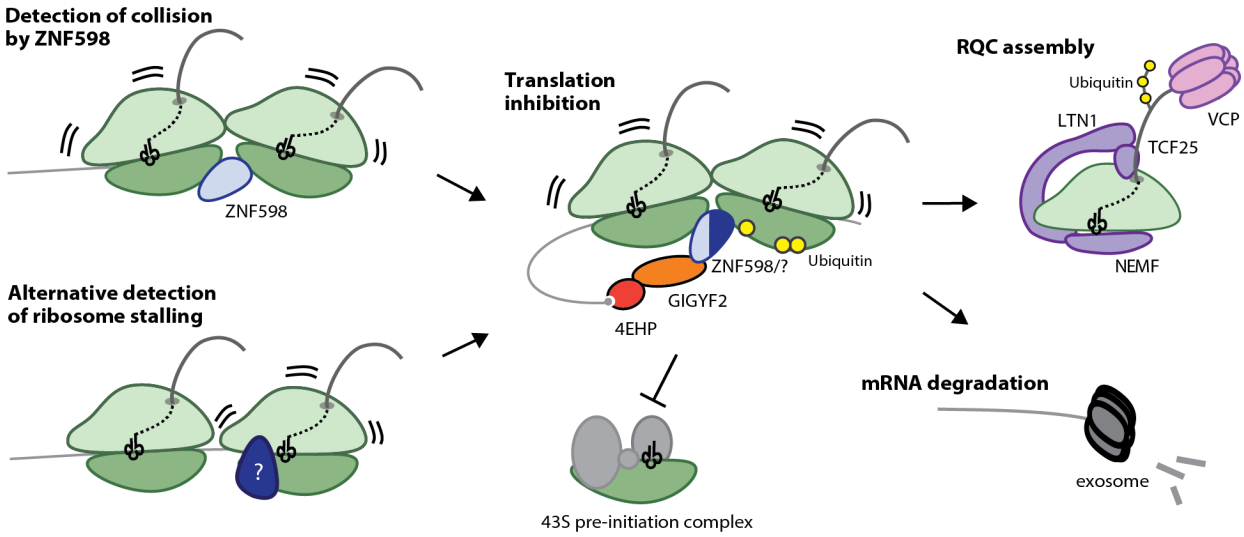

Figure 33. Model of translation shut-off upon ribosome stalling. Ribosome collision is detected by the collision sensor ZNF598. Its binding triggers a cascade of events that ultimately leads to the release of the stalled ribosome, and the degradation of the faulty mRNA and stalled nascent peptide. In addition, ZNF598 recruits the translation inhibitors GIGYF2 and 4EHP to the defective message, which blocks further ribosome initiation. Recruitment of GIGYF2 and 4EHP to defective messages could be mediated by factors other than ZNF598.

3. DISCUSSION

The cell faces an inherent challenge in detecting problematic mRNAs in that it is only through the act of translation itself that the lesion can be recognized, and failure of this recognition results in cytotoxicity. Our work reveals a novel mechanism in which failed translation leads to inhibition of further translation initiation on that message. This pathway acts in parallel with previously described quality control pathways, which trigger mRNA degradation, ribosome release, and proteasomal degradation of the stalled nascent polypeptide. Without a mechanism to block further initiation on problematic messages, translation of faulty mRNAs would continue for as long as the message persists. GIGYF2 and 4EHP enable the cell to break this cycle by allowing a failed translation event to initiate a specific negative feedback loop which shuts down further translation of the message. Although GIGYF2 and 4EHP have been implicated in translational control in a number of different settings (Amaya Ramirez et al., 2018; Fu et al., 2016; Kryszke et al., 2016; Morita et al., 2012; Peter et al., 2017; Tollenaere et al., 2019), our data argue that faulty mRNAs that cause ribosome stalling comprise an important subset of endogenous substrates for GIGYF2 and 4EHP mediated repression. Indeed, loss of GIGYF2 specifically increases translational output from two distinct classes of stalling reporters. Moreover, knocking down GIGYF2 in combination with loss of RQC components had a strong synergistic growth interaction in the absence of a reporter, suggesting that there is a continuous production of endogenous stalling substrates that engage RQC.

How then are stalled ribosomes recognized and how is GIGYF2 recruited? Recruitment of GIGYF2 and 4EHP to their endogenous substrate is hypothesized to occur via sets of auxiliary RNA binding proteins that serve as adapters. Our data argue that ZNF598 can serve as one such adapter to recruit the inhibitory complex to defective messages. However, GIGYF2 and 4EHP

are still capable of repressing translation initiation on faulty mRNAs even in a ZNF598 null background (Fig. 7B, C). These data suggest that there are both ZNF598-dependent and ZNF598-independent mechanisms for recruitment of GIGYF2 and 4EHP to mediate translation inhibition on defective messages (Fig. 7D). The identity of these additional adapters and whether they are redundant with ZNF598, activated or expressed as a compensatory mechanism upon ZNF598 loss, or act on specific classes of faulty mRNAs remains to be explored.

How is translation initiation inhibited? Since 4EHP is a cap binding protein, one might naively expect that GIGYF2 and 4EHP will exclusively affect cap-dependent translation. However, further considerations suggest that GIGYF2 and 4EHP may have a broader effect on translation. For example, GIGYF2 contains a Glycine/Tryptophan (GW)-rich motif that has been shown to facilitate phase transition (Sheu-Gruttadauria and MacRae, 2018). Thus, an attractive hypothesis is that upon stalling, messages bound by GIGYF2 are sequestered away in an inhibitory environment that further interferes with translation, in addition to the direct inhibitory effect of 4EHP-mediated cap sequestration. In support of this hypothesis, using single mRNA imaging in live cells Moon and colleagues (Moon et al., 2020) observed that messages that contain stalled ribosomes can partition into stress granules under different cellular conditions. As a result, the molecular mechanism by which GIGYF2 and 4EHP mediate translational repression upon ribosome stalling is likely multidimensional and remains to be fully explored.

Regardless of their recruitment or silencing mechanism, our data establish a critical role for GIGYF2 and 4EHP in inhibiting translation initiation on defective mRNAs. The synergistic growth defects with core RQC components highlight the importance of these two factors in preventing accumulation of incomplete proteins. Loss of GIGYF2 has been associated with neurodegenerative and neurodevelopmental phenotypes (Krumm et al., 2015; Thyme et al.,

2019), similar to loss of RQC components (Chu et al., 2009). It is tempting to speculate that dysregulation of the GIGYF2/4EHP pathway increases the burden on the proteostasis network in neurons. As these cells age, they can either accumulate defective mRNAs or become less efficient in detecting and/or coping with stalled ribosomes. If these cells lack functional GIGYF2 and 4EHP to translationally silence such defective messages, the increased stalling burden may overwhelm the RQC pathway in cells leading to cell stress and neurodegenerative disease.

4. MATERIALS AND METHODS

4.1. Yeast Strains

All strains used in this study are listed in Table 1. Strain BY4741 was used as the wild-type parental strain. Genomic knockouts were generated by one-step gene replacement. The knockouts were confirmed by genomic PCR. Rqc2p^{mut} strain was generated by replacing the endogenous *RQC2* open reading frame with the mutant version via scarless pop-in/pop-out method. Stalling constructs (GFP_{20Lys}, $GFP_{Lys\text{-}free}$, XTEN0-80, $His3_{Lys\text{-}free}$) were expressed on yeast centromeric plasmids. Rqc2p constructs were overexpressed from yeast episomal plasmids.

4.2. Immunoprecipitation and western blot in yeast

Cells were grown to final OD_{600} between 0.6 and 1 and harvested by centrifugation. The pellets were washed once in water and resuspended in yeast lysis buffer (10 mM Tris pH7.5, 150 mM NaCl, 0.5 mM EDTA, 0.5% NP-40, 1X Halt^{TM}Protease Inhibitor Cocktail (Thermo Fisher Scientific)). An equal volume of glass beads (BioSpec, 0.5 mm, acid washed) was added to the cells and the cells were lysed by vortexing for 1 min and chilling on ice for 1 min, five times total. The lysate was clarified by centrifugation at 20,000 g for 2 min. Protein concentration was measured with BCA Assay (Thermo Fisher Scientific).

Cell lysates were denatured at 70°C for 10 min in 1X Laemmli buffer with β-Mercaptoethanol (BME). Proteins were separated on Bolt® 4-12% Bis-tris gels (Thermo Fisher Scientific), transferred to nitrocellulose membrane using the Trans-Blot® Turbo™ Transfer System (Bio-Rad) according to the manufacturer's instructions, blocked with 5% milk in TBS, and subsequently probed. The HA epitope tag was detected using the high-affinity rat anti-HA

antibody (Roche 3F10, 1:1,000 dilution). The FLAG epitope tag was detected using the high-affinity mouse anti-FLAG antibody (Sigma F1804, 1:3,000 dilution). Hexokinase was detected using the rabbit anti-hexokinase antibody (United States Biological **H2035-02,** 1:10,000 dilution). Licor IRDye700 anti-mouse (Odyssey), IRDye800/IRDye700 anti-rabbit (Odyssey), or IR800 anti-rat (Rockland) secondary antibodies were then used at 1:10,000 dilution. All blots were visualized using the Licor (Odyssey) system. ImageJ was used for protein quantification. All samples were normalized to Hexokinase loading control.

4.3. *in vivo* ubiquitin assay

Myc-tagged ubiquitin was expressed ectopically under a copper-inducible promoter (Table 2). Yeast cells were grown for 2 h in the presence of 200 μM Cu_2SO_4 to induce Myc-Ubiquitin expression. MG132 proteasome inhibitor was added at 60 μM final concentration. After 1 h, cells were harvested via centrifugation. Yeast cells were treated with 0.1 M NaOH for 5 min at room temperature, pelleted, resuspended and boiled in the presence of 1% SDS, 50 mM Tris-HCl pH 7.5, 5 mM EDTA, 5 mM N-ethylmaleimide (NEM) and 1X Halt™ Protease Inhibitor Cocktail (Thermo Fisher Scientific). 100 μl of boiled lysate was further diluted with 900 μl of IP buffer (50 mM Tris-HCl pH 7.5, 250 mM NaCl, 5 mM EDTA, 0.5% NP40, 1 mM NEM), and incubated with 25 ul bead-conjugated anti-Flag antibody (Anti-FLAG® M2 Magnetic Beads, Sigma-Aldrich) or 20 ul bead-conjugated anti-HA antibody (Pierce™ Anti-HA Magnetic Beads, Thermo Fisher Scientific) for 2 h at room temperature. After three washes in IP buffer, beads were boiled in 2X Laemmli Buffer with no BME, and the eluates were used for immunoblot.

4.4. Mammalian cell culture and cell line generation

K562 cells were grown in RPMI-1640 with 25mM HEPES, 2.0 g/L NaHCO3, 0.3 g/L L-Glutamine supplemented with 10% FBS, 2 mM glutamine, 100 units/mL penicillin and 100 µg/mL streptomycin. HEK293T cells were grown in Dulbecco's modified eagle medium (DMEM) in 10% FBS, 2 mM glutamine, 100 units/mL penicillin and 100 µg/mL streptomycin.

Reporter constructs ($GFP_{Non\text{-}stop}$, GFP_{Stop}, GFP_{PolyA}, K20, $RFP_{Non\text{-}stop}$, RFP_{Stop}, $GFP_{MS2\text{-}stop}$, MS2BP, MS2BP-ZNF598, MS2BP-GIGYF2, MS2BP-4EHP) were stably transduced into K562 CRISPRi cell line (Horlbeck et al., 2016) using Piggy-Bac transposition (System Biosciences PB210PA-1 and corresponding Piggy-Bac expression vector Table 4). Positive cells were isolated by FACS on a BD FACSAria2.

Transient expression of reporters ($GFP_{Non\text{-}stop}$, GFP_{Stop}, GFP_{PolyA}, MS2BP, MS2BP-ZNF598, MS2BP-GIGYF2, MS2BP-4EHP) was achieved by transfecting HEK293T cells with vectors from Table 4 using TransIT-LTI Transfection Reagent (Mirus, MIR 2306) according to the manufacturer's instructions.

Individual gene knockdowns were carried out by selecting sgRNA protospacers from compact hCRISPRi-v2 library and ligating them into lentiviral plasmid pU6-sgRNA EF1α-puro-t2a-BFP (Addgene 60955) as previously described (Horlbeck et al., 2016), or using a similar vector where the BFP marker was replaced with RFP. Protospacer sequences used for individual knockdowns are listed in Table 5. The resulting sgRNA expression vectors were packaged into lentivirus by transfecting HEK293T with standard packaging vectors using TransIT-LTI Transfection Reagent (Mirus, MIR 2306). The viral supernatant was harvested 2–3 days after transfection and filtered through 0.45 µm PVDF filter and/or frozen prior to transduction into CRISPRi knockdown cell lines described above.

GFP11-GIGYF2 tagged HEK293T cells were generated as previously described (Leonetti *et al*., PNAS, 2016), using targeting sgRNA (AATACGGAACAGAATGGCAG) and ssDNA oligo(TATTTTTCTCGTTAACAGGTTTCTTCACATATAAAAATCTATTGTAAAAATACGGAAAAGAatgcgtgaccacatggtccttcatgagtatgtaaatgctgctgggattacaGGCGGTGGAGGGAGTggcggaggtGGATCCGCAGCGGAAACGCAGACACTGAACTTTGGGCCTGAATGGTGAGTTTTCAAAATCTCAT).

ZNF598 knockout cell line was generated by transfecting K562 CRISPRi cells with an all-in-one vector pSpCas9(BB)-2A-GFP (PX458) (Addgene plasmid #48138). This vector was modified to express two sgRNAs targeting ZNF598 [ACCGCTGCTCTACCAAGATG], [ATGGGGACTTTGCCTCACTG]. Three days post transfection, GFP positive cells were sorted into single cells. These clones were expanded and ZNF598 knockout was confirmed by western blot for protein expression (Bethyl Laboratories, A305-108A-T), and genotyped with Genewiz amplicon-ez sequencing. The CRISPR-Cas9 induced genome edits were identified by using the knock-knock computational pipeline developed by Canaj and colleagues.

4.5. Genome-scale CRISPRi screening

Genome-scale screens were conducted similar to previously described screens (Gilbert et al., 2014; Horlbeck et al., 2016). The CRISPRi compact library (5 sgRNA/TSS) CRISPRi-v2 (Addgene, Cat#83969) were transduced in duplicate into K562 CRISPRi cells at MOI < 1 (percentage of transduced cells 2 days after transduction: 20%–40%). Replicates were maintained separately in 1.5 L of RPMI-1640 in 3 L spinner flasks for the course of the screen. 2 days after transduction, the cells were selected with 1 mg/mL puromycin for 2 days, until transduced cells accounted for 80%–95% of the population. The cells were maintained in spinner

flasks by daily dilution to $0.5 \cdot 10^6$ cells /mL at an average coverage of greater than 500 cells per sgRNA for the duration of the screen. Genomic DNA was isolated from frozen cells, and the sgRNA-encoded regions were enriched, amplified, and prepared for sequencing as described previously (Gilbert et al., 2014).

FACS based screen

Cells were sorted using BD FACS Aria2 2 days after recovery from puromycin selection based on GFP fluorescence of $GFP_{Non\text{-}stop}$ reporter. Cells with the highest (~30%) and lowest (~30%) GFP expression were collected and immediately frozen. Approximately 30 million cells were collected per group.

Growth based Screen

K562 CRISPRi cells were infected with control sgRNA or sgRNA targeting *NEMF* that expressed RFP as a marker. RFP positive cells were sorted on a BD FACSAria2. Both cell lines were infected with the hCRISPR-v2 library. 100,000 cells from both cell lines were harvested after recovery from puromycin selection as Day 0, and then again after 10 doublings.

Screen analysis

Sequencing reads were aligned to the CRISPRi v2 library sequences, counted, and quantified using the Python-based ScreenProcessing pipeline (https://github.com/mhorlbeck/ScreenProcessing; Horlbeck et al., 2016). Generation of negative control genes and calculation of phenotypes and Mann-Whitney p-values was performed as described previously (Gilbert et al., 2014; Horlbeck et al., 2016). GFP phenotypes were calculated from the top 30% GFP sorted samples, divided by the bottom 30% GFP. Phenotypes from sgRNAs targeting the same gene were collapsed into a single GFP stabilization phenotype using the average of the top three scoring sgRNAs (by absolute value) and assigned a p-value

using the Mann-Whitney test of all sgRNAs targeting the same gene compared to the non-targeting controls. All additional CRISPRi screen data analyses were performed in Python 2.7 using a combination of Numpy (v1.12.1), Pandas (v0.17.1), and Scipy (v0.17.0). For all experiments, details of quantification and statistical methods used are described in the corresponding figure legends or results sections.

4.6. Individual evaluation of sgRNA phenotypes

Single sgRNA expression vectors were individually cloned by annealing complementary synthetic oligonucleotide pairs (Integrated DNA Technologies) for each sgRNA with flanking BstXI and BlpI restriction sites and ligating the resulting double-stranded segment into either BstXI/BlpI-digested pCRISPRi-v2 (marked with a puromycin resistance cassette and BFP similar to Horlbeck et al., 2016) or BstXI/BlpI-digested pU6-sgRNA EF1a-puro-t2a-mCherry (marked with a puromycin resistance cassette and RFP).

Dual sgRNA expression vectors were assembled by a two-step cloning procedure. First, sgRNAs to be included were cloned into the corresponding individual sgRNA expression vectors. sgRNAs destined for the first position of the dual sgRNA vector were cloned into either pMJ002 or pCRISPRia-v2 (Addgene #84832), which both contain a mU6 promoter for sgRNA expression, and sgRNAs destined for the second position were cloned into pMJ003, which contains a hU6 promoter for sgRNA expression. All vectors contain the same constant region and pMJ002 and pMJ003 contain specific primer binding sites flanking the sgRNA expression cassette. Complementary oligonucleotides (Integrated DNA Technologies) containing the sgRNA sequence and ligation overhangs were annealed and ligated into the corresponding BstXI/BlpI-digested sgRNA expression vectors. Single clones from this procedure were used as

templates for the second assembly step, in which the sgRNA expression cassettes containing the U6 promoter, sgRNA sequence, and constant region were assembled into a vector backbone containing a puromycin resistance marker and BFP (pCRISPRia-v2 [Addgene #84832]) or mCherry (a version of pU6-sgCXCR4-2 [Addgene #46917] modified to include a BlpI site). The desired sgRNA expression cassettes were PCR-amplified (pMJ002-based constructs: oMJ0767 [GTTAGTACCGGGCCCGC] and oMJ0768 [CCATAGCTGAGTGTAGATTCGAGCAAAAAAAGCACCGACTCGG]; pCRISPRia-v2-based constructs: oMJ0873 [CCAGTTTGGTTAGTACCGGGCCCGCTCTAGAGATCCGACGCGC] and oMJ0768; pMJ003-based constructs: oMJ0612 [GCTCGAATCTACACTCAGCTATGG] and oMJ0613 [GCCGCCTAATGGATCCTAG]) and inserted into XbaI/XhoI-digested backbone by a single three-piece Gibson assembly step.

Protospacer sequences used for individual evaluation are listed in Table 5. The resulting sgRNA expression vectors were individually packaged into lentivirus. These sgRNA vectors were transduced into K562-dCas9 cells expressing $GFP_{Non\text{-}stop}$ at MOI < 1 (20 – 40% infected cells). BFP and GFP protein levels were measured by flow cytometry at day 5 post infection. Median fluorescent values were calculated for each cell line using FlowJo software and compared fluorescent levels after sgRNA knockdown to a cell line expressing to a non-targeting sgRNA.

Internally controlled growth assays:

Dual sgRNA growth phenotypes were performed by transducing cells with dual sgRNA expression constructs at MOI < 1 (15 – 30% infected cells). The fraction of sgRNA-expressing cells was measured from 4-16 days after infection by flow cytometry on an LSR-II (BD

Biosciences). A population of infected cells was selected to purity with puromycin (1 mg/mL), allowed to recover for 1 day, and harvested for measurement of mRNA levels by RT-qPCR (see below). Experiments were performed in duplicate from the infection step. The expected double phenotype score was calculated by adding the phenotype of both sgRNAs on day 16. Epistasis was measured by subtracting the expected phenotype from the measured phenotype of dual knockdowns.

4.7. Ribosome profiling and RNA sequencing

Ribosome Profiling:

K562-dCas9 cell line stably expressing $GFP_{Non\text{-}stop}$ was infected with lenti vectors containing a guide RNA against one gene or non-targeting guide RNA (Table 5). Cells were selected using FACS to recover cells containing sgRNA (labeled with RFP). Cyclohexamide was added (100mg/ul) to the cells and they were incubated for 5 minutes at 37 °C and then pelleted at 400g for 5 minutes. Media was removed and cell pellets were immediately snap frozen. Libraries were prepared according to McGlincy and Ingolia, Methods, 2017.

RNA sequencing:

RNA was extracted using Zymo mini RNA prep (R2053) and libraries were cloned using Illumnia true stranded total RNA seq kit (20020596).

Ribosome profiling and RNAseq analysis:

Ribosome profiling and RNA-seq libraries were sequenced on an Illumina HiSeq 4000 as single end 50-bp reads (UCSF Center for Advanced Technology) at a depth of 22-64 million reads per library. Ribosome profiling reads were processed by removing 3' linker sequences using *FASTX clipper* and de-multiplexed using *FASTX barcode splitter*

(http://hannonlab.cshl.edu/fastx_toolkit/). Sample barcodes and unique molecular identifiers were trimmed using a custom Python script. Next, abundant reads were filtered by aligning to a custom library of human rRNAs, tRNAs, and primer sequences using *bowtie* v1.2 (http://bowtie-bio.sourceforge.net/). All remaining reads were aligned to a modified human genome (GRCh38.92 with addition of our CRISPRi construct and the $GFP_{Non\text{-}stop}$) using *tophat* v2.1.1 (https://ccb.jhu.edu/software/tophat/; relevant parameters: --read-mismatches=1 and --no-novel-juncs). After alignment, uniquely mapping reads were extracted, and *plastid* (https://plastid.readthedocs.io) was used to obtain gene-level read counts and normalized counts, reads per kilobase per million mapped reads (RPKM). To assign reads to genomic positions, a p-site offset of 12 nucleotides was determined by calculating the average distance of the start codon peak from the start codon (*plastid psite*). To assess the quality of the ribosome profiling data, we confirmed that the aligned reads displayed the expected three nucleotide periodicity (phasing) and that the majority of ribosome footprints had a length of 28-31 bp for all libraries. We also confirmed that the CRISPRi system produced robust target knockdown on the day of the experiment at the level of ribosome footprints (knockdown of target genes >88% for all genes). The RNA-seq libraries were processed using the same pipeline as the ribosome profiling libraries, with the exception that *tophat* was run with –read-mismatches=2 due to the longer RNAseq read length. All downstream analyses were performed using the Python libraries pandas, plastid, matplotlib, seaborn, numpy, and scipy.

For Figure 12A footprints from K562 CRISPRi cells bearing non-targeting sgRNA are plotted as reads per million. Here, we plotted all aligned reads rather than uniquely aligned reads to visualize read density in the $GFP_{Non\text{-}stop}$ MALAT1 triple helix, which is identical to the endogenous MALAT1 lncRNA. To confirm that the reads aligning to the MALAT1 triple helix

in the $GFP_{Non\text{-}stop}$ are not derived from the endogenous MALAT1 lncRNA, we performed ribosome profiling in a K562 CRISPRi cell line without the $GFP_{Non\text{-}stop}$ reporter. Here, we found that the endogenous MALAT1 background rate was <10% of the $GFP_{Non\text{-}stop}$ footprints in the MALAT1 triple helix, suggesting that the $GFP_{Non\text{-}stop}$ triple helix is indeed translated. For Figure 19C translational efficiencies were calculated by normalizing the $GFP_{Non\text{-}stop}$ GFP ribosome footprint rpm to the $GFP_{Non\text{-}stop}$ RNAseq rpm.

4.8. RT-qPCR

Total RNA was isolated from frozen cell samples using TRIzol reagent (Thermo Fisher Scientific) and Phase Lock Gel tubes (VWR), treated with Turbo DNase (Thermo Fisher Scientific), or using Direct-zol RNA MiniPrep kit. Reverse-transcription was carried using M-MLV (Thermo Fisher Scientific) or SSIII Reverse-transcriptase (Thermo Fisher Scientific) with random hexamer primers (Thermo Fisher Scientific, SO124) in the presence of RNaseIN Recombinant Ribonuclease Inhibitor (Thermo Fisher Scientific). Quantitative PCR (qPCR) was performed with Kappa Sybr Fast qPCR 2x Mix (Roche), according to the manufacturer's instructions on a LightCycler 480 Instrument (Roche). Experiments were performed in technical triplicates. RT-qPCR primers used are listed in (Table 6).

4.9. Immunoprecipitation and western blot in mammalian cell culture

Cells were lysed in buffer containing 10mM Tris 7.5, 150 mM NaCl, 0.5% NP-40, 5 mM Mg_2Cl, and 1x Halt™ Protease Inhibitor Cocktail (Thermo Fisher Scientific). The lysates were cleared by centrifugation at 20,000 x g for 10 min and bound to GFP-Trap Magnetic Beads (Chrometech) for 2h at 4 °C. Beads were washed 3 times with IP Buffer (10mM Tris 7.5, 150

mM NaCl, 0.1% NP-40, 5 mM Mg_2Cl). Bound material was eluted by boiling in Laemmli Buffer for 10 min at 90°C.

Proteins were separated on Bolt® 4-12% Bis-tris gels (Thermo Fisher Scientific), transferred to PVDF membrane using the Mini Trans-Blot Cell (Bio-Rad) according to the manufacturer's instructions, blocked with 5% milk in TBS, and subsequently probed. Rabbit anti ZNF598 antibody (Bethyl Laboratories, A305-108A-T), rabbit anti GIGYF2 antibody (Bethyl Laboratories, A303-731A-M), and rabbit anti 4EHP antibody (Cell Signaling, 6916S) primary antibodies were used. LI-COR IRDye800/IRDye700 anti-rabbit (Odyssey) secondary antibody was used at 1:10,000 dilution. All blots were visualized using the LI-COR (Odyssey) system.

4.10. ZNF598 Mass Spectrometry

Cell lines

3X-FLAG-tagged ZNF598 overexpressing (ZNF598-OE) Flp-In T-Rex 293 cells (kind gift from Dr. Nahum Sonenberg and Dr. Thomas Tuschl, Garzia *et al.*, Nature Communications, 2017) were grown in high-glucose Dulbecco's Modified Eagle Medium (Thermo Fisher, 11995040, containing 4 mM L-Glutamine and 1 mM sodium pyruvate) supplemented with 10% (v/v) fetal bovine serum. The affinity purification mass spectrometry experiment was performed in biological triplicate. Two million low-passage cells were seeded per 10 cm dish. Expression of 3X-FLAG-tagged ZNF598 was induced (24 hours post seeding) for 24 hours by the addition of doxycycline at 1 μg/ml at final concentration.

FLAG-immunoprecipitation of 3X-FLAG-ZNF598 from HEK293 cells

Cells were washed with warm PBS (containing 360 μM emetine), and harvested in ice-cold lysis buffer (50 mM TRIS pH 8.0, 150 mM KCl, 15 mM $MgCl_2.6H_2O$, 5% glycerol)

supplemented with 1% Triton X-100, 360 µM emetine, 20 mM N-ethylmaleimide, 80 units TURBO DNase (Thermo Fisher, AM2238) and protease inhibitors (cOmplete Protease Inhibitor Cocktail, Roche; Protease Inhibitor Cocktail, Millipore Sigma; and PMSF, Millipore Sigma). Cell lysates were clarified in a tabletop micro-centrifuge (15 minutes, 4°C). Equal protein amounts from the clarified supernatant were used for each immunoprecipitation. The clarified supernatant was incubated with ANTI-FLAG-Agarose M2 affinity gel (Millipore Sigma #A2220, 15 µl of packed affinity resin) for 1 hour, washed four times with 400 µl wash 1 buffer (lysis buffer supplemented with 0.1% Triton X-100 and 360 µM emetine), then washed four times with wash 2 buffer (50 mM TRIS pH 8.0, 150 mM KCl, 15 mM $MgCl_2.6H_2O$ supplemented with 360 µM emetine), and eluted in 80 µl elution buffer (50 mM TRIS pH 8.0, 150 mM KCl, 15 mM $MgCl_2.6H_2O$ supplemented with 400 µg/ml 3X FLAG-peptide (Millipore Sigma, #F4799)). Eluates were flash frozen in liquid nitrogen and stored at -80°C prior to protein digestion.

Protein Digestion

Protein extracts (4 µg) were diluted up to 300 µl in 10 mM triethyl ammonium bicarbonate (TEAB) and were reduced with 15 µl of 7.5 mg/ml DL-dithiothreitol (DTT) (60°C, 1 hour). After cooling to room temperature, samples were alkylated with 15 µl of 18.5 mg/ml iodoacetamide for 15 minutes at room temperature in the dark. Reduced and alkylated proteins were buffer-exchanged on a 30 kDa molecular weight spin cartridge (Amicon Ultra 0.5 ml, Millipore Sigma) and washed four times with 400 µl 10 mM TEAB. Proteins were digested overnight at 37°C on the filter with 300 µl Trypsin (20 µg in 3 ml 10 mM TEAB, Promega Sequencing Grade Modified Trypsin). Additional Trypsin (100 µl of 10 mg/ml) was added the

next morning (37°C, 1 hour). Peptides were removed from the top of the filter and the filter was washed twice with 300 2% acetonitrile, 0.1% formic acid. All washes were combined and dried.

Liquid Chromatography and Mass Spectrometry

Liquid Chromatography and Mass Spectrometry was performed at the Mass Spectrometry and Proteomics Core, JHMI. Peptides were analyzed by liquid chromatography interfaced with tandem mass spectrometry (LC/MS/MS) using a Waters nanoACQUITY UPLC system (www.waters.com) interfaced with an Orbitrap Fusion™ Lumos™ Tribrid™ Mass Spectrometer (www.thermofisher.com). Fractions were resuspended in 20 µl loading buffer (2% acetonitrile in 0.1% formic acid) and analyzed by reverse phase liquid chromatography coupled to tandem mass spectrometry. Peptides (50%, approx. 1 µg) were loaded onto a C18 trap (S-10 µM, 120 Å, 75 µm x 2 cm, YMC, Japan) and subsequently separated on an in-house packed PicoFrit column (75 µm x 200 mm, 15u, +/-1 µm tip, New Objective) with C18 phase (ReproSil-Pur C18-AQ, 3 µm, 120 Å, www.dr-maisch.com) using 2-90% acetonitrile gradient at 300 nl/min over 120 min. Eluting peptides were sprayed at 2.0 kV directly into the Lumos.

Survey scans (full MS) were acquired from 350-1800 m/z with data-dependent monitoring with a 3 sec cycle time. Each precursor individually isolated in a 1.6 Da window and fragmented using HCD activation collision energy 30 and 15 sec dynamic exclusion, first mass being 120 m/z. Precursor and fragment ions were analyzed at resolutions 120,000 and 30,000, respectively, with automatic gain control (AGC) target values at 4e5 with 50 ms maximum injection time (IT) and 1e5 with 100 ms maximum IT, respectively.

Processing of Mass Spectrometry Data

Raw data was processed and analyzed using the MaxQuant software suite (Cox and Mann, Nature Biotechnology, 2008). Default settings were used except that ‘Match between

runs' was turned on to transfer peptide identification from an LC-MS run, in which the peptide has been identified by MS/MS, to another LC-MS run, in which no MS/MS data for the same peptide was acquired or no peptide was assigned (Tyanova *et al.*, Nature Methods, 2016). Search parameters were as follows:

a maximum of two missed cleavages were allowed, cysteine carbamidomethyl was included as a fixed modification, and variable modifications included oxidation of methionine, protein N-terminal acetylation, deamidation of glutamine and asparagine, phosphorylation of serine, threonine and tyrosine, and Gly-Gly ubiquitin remnant on lysine. Database search was performed with Andromeda (Cox and Mann, Nature Biotechnology, 2008; Cox et al., Journal of Proteomic Research, 2011) against Uniprot human database (UP000005640_9606.fasta; downloaded on 09/10/2018) with common serum contaminants and enzyme sequences. False discovery rate (FDR) was set to 1% at both the peptide spectrum match (PSM) and protein level. A minimum peptide count required for protein quantification was set to two. Protein groups were further analyzed using the Perseus software suite (Tyanova *et al.*, Nature Methods, 2016). Common contaminants, reverse proteins and proteins only identified by site were filtered out. LFQ values were transformed to $\log_2$ space and intensity distributions were checked to ensure that data was normally distributed.

Table 1. Yeast strains used in this study.

name	strain	Genotype	source
BY4741	BY4741	*MATa his3Δ1 leu2Δ0 met15Δ0 ura3Δ0*	this study
pdr5Δ	yKK205	BY4741 *pdr5Δ::KanMX*	this study
ltn1Δ	yKK178	BY4741 *ltn1Δ::KanMX*	this study
rqc2Δ	yKK179	BY4741 *rqc2Δ::KanMX*	this study
RQC2mut/ltn1Δ	yKK272	BY4741 *rqc2Δ::RQC2mut ltn1Δ::KanMX*	this study
rqc2Δ/ltn1Δ	yKK287	BY4741 *rqc2Δ::KanMX ltn1Δ::URA3*	this study
RQC2mut	yKK108	BY4741 *rqc2Δ::RQC2mut*	this study
ltn1ΔRING	yKK102	BY4741 *Ltn1ΔRING::NatMX*	Ref. 11
pdr5Δ/ltn1Δ	yKH16	BY4741 *pdr5Δ::Kan ltn1Δ::Nat*	this study
pdr5Δ/rqc2Δ	yKK226	BY4741 *pdr5Δ::Kan rqc2Δ:: Nat*	this study
pdr5Δ/RQC2mut	yKH21	BY4741 *pdr5Δ::Kan rqc2Δ::RQC2mut*	this study
pdr5Δ/ltn1Δ/RQC2mut	yKH22	BY4741 *pdr5Δ::Kan ltn1Δ::Nat rqc2Δ::RQC2mut*	this study
ski2Δ	yKK327	BY4741 *ski2Δ::Ura*	this study
ski2Δ/RQC2mut	yKK328	BY4741 *ski2Δ::Ura rqc2Δ::RQC2mut*	this study
ski2Δ/rqc2Δ	yKK329	BY4741 *ski2Δ::Ura rqc2Δ::Kan*	this study
ski2Δ/ltn1Δ	yKK330	BY4741 *ski2Δ::Ura ltn1Δ::Kan*	this study

Table 2. Yeast plasmids used in this study.

Name	ID	Backbone	Expression	Source
GFP_{20Lys}	pKK148	pRS313	pTDH3-GFP_{20Lys}-3xHA-TEV-R12-RFP	this study
$GFP_{Lys\text{-}free}$	pKK135	pRS313	pTDH3-$GFP_{Lys\text{-}free}$-3xHA-TEV-R12-RFP	this study
GFP_{20Lys} (37 linker)	pKK168	pRS313	pTDH3-GFP_{20Lys}-3xHA-TEV(no linkers) -R12-RFP	this study
GFP_{19Lys} (51 linker)	pKK140	pRS313	pTDH3-GFP_{19Lys}(K238R)-3xHA-TEV-R12-RFP	this study
3xFLAG XTEN0	pKK151	pRS313	pTDH3-$GFP_{Lys\text{-}free}$-3xFlag-TEV-R12-RFP	this study
3xFLAG XTEN10	pKK190	pRS313	pTDH3-$GFP_{Lys\text{-}free}$-3xFlag-XTEN10-TEV-R12-RFP	this study
3xFLAG XTEN20	pKK191	pRS313	pTDH3-$GFP_{Lys\text{-}free}$-3xFlag-XTEN20-TEV-R12-RFP	this study
3xFLAG XTEN40	pKK192	pRS313	pTDH3-$GFP_{Lys\text{-}free}$-3xFlag-XTEN40-TEV-R12-RFP	this study
3xFLAG XTEN80	pKK198	pRS313	pTDH3-$GFP_{Lys\text{-}free}$-3xFlag-XTEN80-TEV-R12-RFP	this study
$His3_{Lys\text{-}free}$	pKK172	pRS316	pTDH3-$His3_{Lys\text{-}free}$-3xHA-TEV-R12-RFP	this study
$His3_{Lys\text{-}free}$ 3xFLAG	pKK175	pRS316	pTDH3-$His3_{Lys\text{-}free}$-3xFlag-TEV-R12-RFP	this study
$His3_{Lys\text{-}free}$ 2xLys	pKK174	pRS316	pTDH3-$His3_{Lys\text{-}free}$-3xHA-2Lys-TEV-R12-RFP	this study
$GFP_{Lys\text{-}free}$ 2xLys	pKK136	pRS313	pTDH3-$GFP_{Lys\text{-}free}$-3xHA-TEV-2Lys-R12-RFP	this study

Name	ID	Backbone	Expression	Source
1K XTEN0	pKK218	pRS313	pTDH3-$GFP_{Lys\text{-}free}$-3xHA-1K-TEV-R12-RFP	this study
1K XTEN10	pKK219	pRS313	pTDH3-$GFP_{Lys\text{-}free}$-3xHA-1K-XTEN10-TEV-R12-RFP	this study
1K XTEN20	pKK220	pRS313	pTDH3-$GFP_{Lys\text{-}free}$-3xHA-1K-XTEN20-TEV-R12-RFP	this study
1K XTEN40	pKK221	pRS313	pTDH3-$GFP_{Lys\text{-}free}$-3xHA-1K-XTEN40-TEV-R12-RFP	this study
2K XTEN20	pKK242	pRS313	pTDH3-$GFP_{Lys\text{-}free}$-3xHA-2K-XTEN20-TEV-R12-RFP	this study
2K XTEN25	pKK243	pRS313	pTDH3-$GFP_{Lys\text{-}free}$-3xHA-2K-XTEN25-TEV-R12-RFP	this study
2K XTEN30	pKK244	pRS313	pTDH3-$GFP_{Lys\text{-}free}$-3xHA-2K-XTEN30-TEV-R12-RFP	this study
2K XTEN35	pKK245	pRS313	pTDH3-$GFP_{Lys\text{-}free}$-3xHA-2K-XTEN35-TEV-R12-RFP	this study
NSD $GFP_{Lys\text{-}free}$	pKK189	pRS313	pTDH3-$GFP_{Lys\text{-}free}$-3xHA_TEV_(AAA)x10_Rz	this study
RQC2	pKK187	pRS426	pPGK-RQC2	this study
RQC2mut	pKK182	pRS426	pPGK-RQC2mut	this study
RQC2-HA	pKK183	pRS426	pPGK-RQC2-HA	this study
RQC2mut-HA	pKK184	pRS426	pPGK-RQC2mut-HA	this study
Myc-Ub	pUb221		pCUP1-3xHis-Myc-Ub	Finley Lab
GFP_{20Lys}-3xFLAG	pKK150	pRS313	pTDH3-GFP_{20Lys}-3xFLAG-TEV-R12-RFP	this study
unfolded GFP	pKK260	pRS313	pTDH3-DHFR-$GFP_{Lys\text{-}free}$(100AA)-3xHA-1K-XTEN40-TEV-R12-RFP	this study

Table 3. Yeast qPCR Primers

Primer	Sequence
GFP F	cgtgaacaaccaccacttca
GFP R	gtctgggtgccctcgtag
ACT1 F	tccgtctggattggtggt
ACT1 R	tgagatccacatttgttggaag

Table 4: Mammalian plasmids used in this study

Name	ID	Backbone	Expression	Source
GFP Non-stop	pKK100	pcDNA3	pCMV-BFP-t2a-GFP-Malat1	this study
GFP Non-stop	pKK122	piggybac	pEIF2a-BFP-T2A-GFP-Malat1	this study
GFP Stop	pKK357	pcDNA3	pCMV-BFP-t2a-GFP-STOP-Malat1	this study
GFP PolyA	pKK358	pcDNA3	pCMV-BFP-t2a-GFP-STOP-polyA	this study
K20	pKH21	piggybac	pEIF2a-BFP-T2A-GFP-K20-RFP	this study
RFP Non-stop	pKH63	piggybac	GFP-pA; RFP-MALAT1	this study
RFP Stop	pKH64	piggybac	GFP-pA; RFP-STOP-MALAT1	this study
yeast control reporter			RFP-pA; GFP-T2A-FLAG-His3	D'Orazio et al., eLife 2019
yeast NGD reporter			RFP-pA; GFP-T2A-FLAG-His3(CGA)12	D'Orazio et al., eLife 2019
GFP MS2-Stop	pKK306	pcDNA	pCMV-3xMS2_BFP-t2a-GFP-stop-stop-Malat1	this study
GFP MS2-Stop	pKK307	piggybac	pEIF2a-3xMS2_BFP-IRES-GFP-stop-stop-Malat1	this study
MS2BP	pKK308	pcDNA	MS2BP-IRES-mCherry	this study
MS2BP-GIGYF2	pKK309	pcDNA	MS2BP-GIGYF2-IRES-mCherry	this study
MS2BP-ZNF598	pKK375	pcDNA3	MS2BP-ZNF598-IRES-mCherry	this study
MS2BP-4EHP	pKK318	pcDNA3	MS2BP-4EHP-IRES-mCherry	this study
MS2BP-ZNF598_C29A	pKK391	pcDNA3	MS2BP-ZNF598_C29A-IRES-mCherry	this study
MS2BP-ZNF598_deltaRING	pKK392	pcDNA3	MS2BP-ZNF598_deltaRING-IRES-mCherry	this study
MS2BP	pKK478	piggybac	MS2BP-IRES-Mcherry	this study
MS2BP-ZNF598_deltaRING	pKK479	piggybac	MS2BP-ZNF598deltaRING-IRES-mCherry	this study
MS2BP-GIGYF2	pKK480	piggybac	MS2BP-GIGYF2-IRES-mCherry	this study
MS2BP-4EHP	pKK481	piggybac	MS2BP-4EHP-IRES-mCherry	this study
MS2BP-ZNF598	pKK482	piggybac	MS2BP-ZNF598WT-IRES-mCherry	this study

Table 5: Protospacers used in this study

Target	sequence
non-targeting 001	GAACGACTAGTTAGGCGTGTAG
NEMF	GAGTACGGCGCGGAGGTCAA
GIGYF2	GGCAGGGGAGCGACACGGAA
4EHP	GCCTGAGGCAGTGGCGACAG
ZNF598	GGCCGGATCCCGGACCATGG
non-targeting 002	GTGTGCAACCTCCGCCGTTGG

Table 6: Mammalian RT-qPCR primers used in this study

Target	forward primer	reverse primer
ZNF598	aaaggtgtacgcattgtacagg	ctccaggtccccgaagag
4EHP	gacaggccacagtgacttcc	gcagccgaataatccacttg
GIGYF2	tctgtgggtcaggaatttgg	gacatctgaccacaaccaaaga
Actin	gctacgagctgcctgacg	ggctggaagagtgcctca
GFP_1	tgaccacatggtccttcttg	atagttcatccatgccatgtgta
GAPDH	acgggaagcttgtcatcaat	catcgccccacttgatttt
RFP	cccgtaatgcagaagaagacc	gcttgatctcgcccttca
GFP_2	gtggatggcgctcttgaa	cgacggcggctactacag
NEMF	ctatatgaaaacaacatccaacttcag	cgtcagtatgtcttcaactggttt

5. REFERENCES

Akimitsu, N., Tanaka, J., and Pelletier, J. (2007). Translation of nonSTOP mRNA is repressed post-initiation in mammalian cells. EMBO J. *26*, 2327–2338.

Amaya Ramirez, C.C., Hubbe, P., Mandel, N., and Béthune, J. (2018). 4EHP-independent repression of endogenous mRNAs by the RNA-binding protein GIGYF2. Nucleic Acids Res.

Ash, M.R., Faelber, K., Kosslick, D., Albert, G.I., Roske, Y., Kofler, M., Schuemann, M., Krause, E., and Freund, C. (2010). Conserved β-hairpin recognition by the GYF domains of Smy2 and GIGYF2 in mRNA surveillance and vesicular transport complexes. Structure *18*, 944–954.

Ban, N., Nissen, P., Hansen, J., Moore, P.B., and Steitz, T.A. (2000). The Complete Atomic Structure of the Large Ribosomal Subunit at 2.4 Å Resolution. Science (80-.). *289*.

Bengtson, M.H., and Joazeiro, C.A.P. (2010). Role of a ribosome-associated E3 ubiquitin ligase in protein quality control. Nature *467*, 470–473.

Bertrand, E., Chartrand, P., Schaefer, M., Shenoy, S.M., Singer, R.H., and Long, R.M. (1998). Localization of ASH1 mRNA Particles in Living Yeast. Mol. Cell *2*, 437–445.

Brandman, O., and Hegde, R.S. (2016). Ribosome-associated protein quality control. Nat. Struct. Mol. Biol. *23*.

Brandman, O., Stewart-Ornstein, J., Wong, D., Larson, A., Williams, C.C., Li, G.-W., Zhou, S., King, D., Shen, P.S., Weibezahn, J., et al. (2012). A ribosome-bound quality control complex triggers degradation of nascent peptides and signals translation stress. Cell *151*, 1042–1054.

Canaj, H., Hussmann, J.A., Li, H., Beckman, K.A., Goodrich, L., Cho, N.H., Li, Y.J., Santos, D.A., McGeever, A., Stewart, E.M., et al. (2019). Deep profiling reveals substantial heterogeneity of integration outcomes in CRISPR knock-in experiments. BioRxiv 841098.

Choe, Y.-J., Park, S.-H., Hassemer, T., Körner, R., Vincenz-Donnelly, L., Hayer-Hartl, M., and Hartl, F.U. (2016). Failure of RQC machinery causes protein aggregation and proteotoxic

stress. Nature *531*, 191–195.

Chu, J., Hong, N.A., Masuda, C.A., Jenkins, B. V., Nelms, K.A., Goodnow, C.C., Glynne, R.J., Wu, H., Masliah, E., Joazeiro, C.A.P., et al. (2009). A mouse forward genetics screen identifies LISTERIN as an E3 ubiquitin ligase involved in neurodegeneration. Proc. Natl. Acad. Sci. *106*, 2097–2103.

D'Orazio, K.N., Wu, C.C.-C., Sinha, N., Loll-Krippleber, R., Brown, G.W., and Green, R. (2019). The endonuclease Cue2 cleaves mRNAs at stalled ribosomes during No Go Decay. Elife *8*.

Defenouillère, Q., Yao, Y., Mouaikel, J., Namane, A., Galopier, A., Decourty, L., Doyen, A., Malabat, C., Saveanu, C., Jacquier, A., et al. (2013). Cdc48-associated complex bound to 60S particles is required for the clearance of aberrant translation products. Proc. Natl. Acad. Sci. U. S. A. *110*, 5046–5051.

Defenouillère, Q., Zhang, E., Namane, A., Mouaikel, J., Jacquier, A., and Fromont-Racine, M. (2016). Rqc1 and ltn1 prevent c-terminal alanine-threonine tail (cat-tail)-induced protein aggregation by efficient recruitment of cdc48 on stalled 60s subunits. J. Biol. Chem. *291*, 12245–12253.

Dimitrova, L.N., Kuroha, K., Tatematsu, T., and Inada, T. (2009). Nascent peptide-dependent translation arrest leads to Not4p-mediated protein degradation by the proteasome. J. Biol. Chem. *284*, 10343–10352.

Doma, M.K., and Parker, R. (2006). Endonucleolytic cleavage of eukaryotic mRNAs with stalls in translation elongation. Nature *440*, 561–564.

Engel, S.R., Dietrich, F.S., Fisk, D.G., Binkley, G., Balakrishnan, R., Costanzo, M.C., Dwight, S.S., Hitz, B.C., Karra, K., Nash, R.S., et al. (2014). The reference genome sequence of Saccharomyces cerevisiae: then and now. G3 *4*, 389–398.

Frischmeyer, P.A., Van Hoof, A., O'Donnell, K., Guerrerio, A.L., Parker, R., and Dietz, H.C. (2002). An mRNA surveillance mechanism that eliminates transcripts lacking termination codons. Science (80-.).

Fu, R., Olsen, M.T., Webb, K., Bennett, E.J., and Lykke-Andersen, J. (2016). Recruitment of the 4EHP-GYF2 cap-binding complex to tetraproline motifs of tristetraprolin promotes

repression and degradation of mRNAs with AU-rich elements. RNA *22*, 373–382.

Garzia, A., Jafarnejad, S.M., Meyer, C., Chapat, C., Gogakos, T., Morozov, P., Amiri, M., Shapiro, M., Molina, H., Tuschl, T., et al. (2017). The E3 ubiquitin ligase and RNA-binding protein ZNF598 orchestrates ribosome quality control of premature polyadenylated mRNAs. Nat. Commun. *8*.

Gilbert, L.A., Horlbeck, M.A., Adamson, B., Villalta, J.E., Chen, Y., Whitehead, E.H., Guimaraes, C., Panning, B., Ploegh, H.L., Bassik, M.C., et al. (2014). Genome-Scale CRISPR-Mediated Control of Gene Repression and Activation. Cell *159*, 647–661.

Hashimoto, S., Sugiyama, T., Yamazaki, R., Nobuta, R., and Inada, T. (2020). Identification of a novel trigger complex that facilitates ribosome-associated quality control in mammalian cells. Sci. Rep. *10*, 1–12.

Higgins, R., Gendron, J.M., Rising, L., Mak, R., Webb, K., Kaiser, S.E., Zuzow, N., Riviere, P., Yang, B., Fenech, E., et al. (2015). The Unfolded Protein Response Triggers Site-Specific Regulatory Ubiquitylation of 40S Ribosomal Proteins. Mol. Cell *59*, 35–49.

Horlbeck, M.A., Gilbert, L.A., Villalta, J.E., Adamson, B., Pak, R.A., Chen, Y., Fields, A.P., Park, C.Y., Corn, J.E., Kampmann, M., et al. (2016). Compact and highly active next-generation libraries for CRISPR-mediated gene repression and activation. Elife *5*.

Ikeuchi, K., Tesina, P., Matsuo, Y., Sugiyama, T., Cheng, J., Saeki, Y., Tanaka, K., Becker, T., Beckmann, R., and Inada, T. (2019). Collided ribosomes form a unique structural interface to induce Hel2-driven quality control pathways. EMBO J. *38*.

Ito-Harashima, S., Kuroha, K., Tatematsu, T., and Inada, T. (2007). Translation of the poly(A) tail plays crucial roles in nonstop mRNA surveillance via translation repression and protein destabilization by proteasome in yeast. Genes Dev. *21*, 519–524.

Izawa, T., Tsuboi, T., Kuroha, K., Inada, T., Nishikawa, S. ichi, and Endo, T. (2012). Roles of Dom34:Hbs1 in Nonstop Protein Clearance from Translocators for Normal Organelle Protein Influx. Cell Rep. *2*, 447–453.

Juszkiewicz, S., and Hegde, R.S. (2017). Initiation of Quality Control during Poly(A) Translation Requires Site-Specific Ribosome Ubiquitination. Mol. Cell *65*, 743-750.e4.

Juszkiewicz, S., Chandrasekaran, V., Lin, Z., Kraatz, S., Ramakrishnan, V., and Hegde, R.S. (2018). ZNF598 Is a Quality Control Sensor of Collided Ribosomes Correspondence. Mol. Cell *72*, 469–481.

Klauer, A.A., and van Hoof, A. (2012). Degradation of mRNAs that lack a stop codon: A decade of nonstop progress. Wiley Interdiscip. Rev. RNA *3*, 649–660.

Kostova, K.K., Hickey, K.L., Osuna, B.A., Hussmann, J.A., Frost, A., Weinberg, D.E., and Weissman, J.S. (2017). CAT-tailing as a fail-safe mechanism for efficient degradation of stalled nascent polypeptides. Science (80-.). *357*.

Koutmou, K.S., Schuller, A.P., Brunelle, J.L., Radhakrishnan, A., Djuranovic, S., Green, R., Arenz, S., Meydan, S., Starosta, A., Berninghausen, O., et al. (2015). Ribosomes slide on lysine-encoding homopolymeric A stretches. Elife *4*, 446–452.

Krumm, N., Turner, T.N., Baker, C., Vives, L., Mohajeri, K., Witherspoon, K., Raja, A., Coe, B.P., Stessman, H.A., He, Z.-X., et al. (2015). Excess of rare, inherited truncating mutations in autism. Nat. Genet. *47*, 582–588.

Kryszke, M.-H., Adjeriou, B., Liang, F., Chen, H., and Dautry, F. (2016). Post-transcriptional gene silencing activity of human GIGYF2.

Letzring, D.P., Dean, K.M., and Grayhack, E.J. (2010). Control of translation efficiency in yeast by codon-anticodon interactions. RNA *16*, 2516–2528.

Letzring, D.P., Wolf, A.S., Brule, C.E., and Grayhack, E.J. (2013). Translation of CGA codon repeats in yeast involves quality control components and ribosomal protein L1. Rna *19*, 1208–1217.

Lytvynenko, I., Paternoga, H., Thrun, A., Balke, A., Müller, T.A., Chiang, C.H., Nagler, K., Tsaprailis, G., Anders, S., Bischofs, I., et al. (2019). Alanine Tails Signal Proteolysis in Bacterial Ribosome-Associated Quality Control. Cell *178*, 76-90.e22.

Lyumkis, D., Oliveira dos Passos, D., Tahara, E.B., Webb, K., Bennett, E.J., Vinterbo, S., Potter, C.S., Carragher, B., and Joazeiro, C.A.P. (2014). Structural basis for translational surveillance by the large ribosomal subunit-associated protein quality control complex. Proc. Natl. Acad. Sci. U. S. A. *111*, 15981–15986.

Malsburg, K. v. d., Shao, S., and Hegde, R.S. (2015). The ribosome quality control pathway can access nascent polypeptides stalled at the Sec61 translocon. Mol. Biol. Cell *26*, 2168–2180.

Matsuo, Y., Ikeuchi, K., Saeki, Y., Iwasaki, S., Schmidt, C., Udagawa, T., Sato, F., Tsuchiya, H., Becker, T., Tanaka, K., et al. (2017). Ubiquitination of stalled ribosome triggers ribosome-associated quality control. Nat. Commun. *8*, 159.

Moon, S.L., Morisaki, T., Stasevich, T.J., and Parker, R. (2020). Coupling of translation quality control and mRNA targeting to stress granules.

Morita, M., Ler, L.W., Fabian, M.R., Siddiqui, N., Mullin, M., Henderson, V.C., Alain, T., Fonseca, B.D., Karashchuk, G., Bennett, C.F., et al. (2012). A Novel 4EHP-GIGYF2 Translational Repressor Complex Is Essential for Mammalian Development. Mol. Cell. Biol. *32*, 3585–3593.

Nissen, P., Hansen, J., Ban, N., Moore, P.B., and Steitz, T.A. (2000). The Structural Basis of Ribosome Activity in Peptide Bond Synthesis. Science (80-.). *289*.

Osuna, B.A., Howard, C.J., KC, S., Frost, A., and Weinberg, D.E. (2017). In vitro analysis of RQC activities provides insights into the mechanism and function of CAT tailing. Elife *6*.

Ozgur, S., Chekulaeva, M., and Stoecklin, G. (2010). Human Pat1b Connects Deadenylation with mRNA Decapping and Controls the Assembly of Processing Bodies. Mol. Cell. Biol. *30*, 4308–4323.

Peter, D., Weber, R., Sandmeir, F., Wohlbold, L., Helms, S., Bawankar, P., Valkov, E., Igreja, C., and Izaurralde, E. (2017). GIGYF1/2 proteins use auxiliary sequences to selectively bind to 4EHP and repress target mRNA expression. Genes Dev. *31*.

Qi, L.S., Larson, M.H., Gilbert, L.A., Doudna, J.A., Weissman, J.S., Arkin, A.P., and Lim, W.A. (2013). Repurposing CRISPR as an RNA-guided platform for sequence-specific control of gene expression. Cell *152*, 1173–1183.

Rom, E., Kim, H.C., Gingras, A.C., Marcotrigiano, J., Favre, D., Olsen, H., Burley, S.K., and Sonenberg, N. (1998). Cloning and characterization of 4EHP, a novel mammalian eIF4E-related cap-binding protein. J. Biol. Chem. *273*, 13104–13109.

Saito, K., Horikawa, W., and Ito, K. (2015). Inhibiting K63 Polyubiquitination Abolishes No-Go Type Stalled Translation Surveillance in Saccharomyces cerevisiae. PLOS Genet. *11*, e1005197.

Schellenberger, V., Wang, C., Geething, N.C., Spink, B.J., Campbell, A., To, W., Scholle, M.D., Yin, Y., Yao, Y., Bogin, O., et al. (2009). A recombinant polypeptide extends the in vivo half-life of peptides and proteins in a tunable manner. Nat. Biotechnol. *27*.

Shao, S., and Hegde, R.S. (2014). Reconstitution of a Minimal Ribosome-Associated Ubiquitination Pathway with Purified Factors. Mol. Cell *55*, 880–890.

Shao, S., Von der Malsburg, K., and Hegde, R.S. (2013). Listerin-dependent nascent protein ubiquitination relies on ribosome subunit dissociation. Mol. Cell *50*, 637–648.

Shao, S., Brown, A., Santhanam, B., and Hegde, R.S. (2015). Structure and Assembly Pathway of the Ribosome Quality Control Complex. Mol. Cell *57*, 433–444.

Shen, P.S., Park, J., Qin, Y., Li, X., Parsawar, K., Larson, M.H., Cox, J., Cheng, Y., Lambowitz, A.M., Weissman, J.S., et al. (2015). Rqc2p and 60S ribosomal subunits mediate mRNA-independent elongation of nascent chains. Science (80-.). *347*, 75–78.

Sheu-Gruttadauria, J., and MacRae, I.J. (2018). Phase Transitions in the Assembly and Function of Human miRISC. Cell *173*, 946-957.e16.

Simms, C.L., Hudson, B.H., Mosior, J.W., Rangwala, A.S., and Zaher, H.S. (2014). An Active Role for the Ribosome in Determining the Fate of Oxidized mRNA. Cell Rep. *9*, 1256–1264.

Simms, C.L., Yan, L.L., Correspondence, H.S.Z., and Zaher, H.S. (2017a). Ribosome Collision Is Critical for Quality Control during No-Go Decay Article Ribosome Collision Is Critical for Quality Control during No-Go Decay. Mol. Cell *68*, 361–373.

Simms, C.L., Thomas, E.N., and Zaher, H.S. (2017b). Ribosome-based quality control of mRNA and nascent peptides. Wiley Interdiscip. Rev. RNA *8*.

Subtelny, A.O., Eichhorn, S.W., Chen, G.R., Sive, H., and Bartel, D.P. (2014). Poly(A)-tail profiling reveals an embryonic switch in translational control. Nature *508*, 66–71.

Sundaramoorthy, E., Leonard, M., Mak, R., Liao, J., Fulzele, A., and Bennett, E.J. (2017).

ZNF598 and RACK1 Regulate Mammalian Ribosome-Associated Quality Control Function by Mediating Regulatory 40S Ribosomal Ubiquitylation. Mol. Cell *65*, 751-760.e4.

Thyme, S.B., Pieper, L.M., Li, E.H., Pandey, S., Wang, Y., Morris, N.S., Sha, C., Choi, J.W., Herrera, K.J., Soucy, E.R., et al. (2019). Phenotypic Landscape of Schizophrenia-Associated Genes Defines Candidates and Their Shared Functions. Cell *177*, 478-491.e20.

Tollenaere, M.A.X., Tiedje, C., Rasmussen, S., Nielsen, J.C., Vind, A.C., Blasius, M., Batth, T.S., Mailand, N., Olsen, J. V., Gaestel, M., et al. (2019). GIGYF1/2-Driven Cooperation between ZNF598 and TTP in Posttranscriptional Regulation of Inflammatory Signaling. Cell Rep. *26*, 3511-3521.e4.

Verma, R., Oania, R.S., Kolawa, N.J., and Deshaies, R.J. (2013). Cdc48/p97 promotes degradation of aberrant nascent polypeptides bound to the ribosome. Elife *2*, e00308.

Wilusz, J.E., JnBaptiste, C.K., Lu, L.Y., Kuhn, C.-D., Joshua-Tor, L., and Sharp, P.A. (2012). A triple helix stabilizes the 3' ends of long noncoding RNAs that lack poly(A) tails. Genes Dev. *26*, 2392–2407.

Yonashiro, R., Tahara, E.B., Bengtson, M.H., Khokhrina, M., Lorenz, H., Chen, K.C., Kigoshi-Tansho, Y., Savas, J.N., Yates, J.R., Kay, S.A., et al. (2016a). The Rqc2/Tae2 subunit of the ribosome-associated quality control (RQC) complex marks ribosome-stalled nascent polypeptide chains for aggregation. Elife *5*.

Yonashiro, R., Tahara, E.B., Bengtson, M.H., Khokhrina, M., Lorenz, H., Chen, K.-C., Kigoshi-Tansho, Y., Savas, J.N., Yates, J.R., Kay, S.A., et al. (2016b). The Rqc2/Tae2 subunit of the ribosome-associated quality control (RQC) complex marks ribosome-stalled nascent polypeptide chains for aggregation. Elife *5*, e11794.

Zuberek, J., Kubacka, D., Jablonowska, A., Jemielity, J., Stepinski, J., Sonenberg, N., and Darzynkiewicz, E. (2007). Weak binding affinity of human 4EHP for mRNA cap analogs.

Publishing Agreement

It is the policy of the University to encourage open access and broad distribution of all theses, dissertations, and manuscripts. The Graduate Division will facilitate the distribution of UCSF theses, dissertations, and manuscripts to the UCSF Library for open access and distribution. UCSF will make such theses, dissertations, and manuscripts accessible to the public and will take reasonable steps to preserve these works in perpetuity.

I hereby grant the non-exclusive, perpetual right to The Regents of the University of California to reproduce, publicly display, distribute, preserve, and publish copies of my thesis, dissertation, or manuscript in any form or media, now existing or later derived, including access online for teaching, research, and public service purposes.

DocuSigned by:
Kelsey Hickey
A6B21DB3E1FD4F1...
Author Signature

5/27/2020
Date